

Channel Estimation for 6G Near-Field Wireless Communications: A Comprehensive Survey

Wen-Xuan Long, *Member, IEEE*, Shengyu Ye, *Graduate Student Member, IEEE*,
 Marco Moretti, *Member, IEEE*, Michele Morelli, *Senior Member, IEEE*,
 Luca Sanguinetti, *Fellow, IEEE*, Rui Chen, *Member, IEEE*, and Cheng-Xiang Wang, *Fellow, IEEE*

Abstract—The sixth-generation (6G) wireless communication systems are expected to evolve toward extremely large aperture arrays (ELAAs), novel antenna architectures, and operation in extremely high-frequency bands to meet the rapidly growing demand for data transmission. The deployment of ELAAs significantly increases the number of antennas, enabling finer spatial resolution and enhanced beamforming capabilities. When operating in extremely high-frequency bands, ELAAs also introduce a fundamental shift in the communication paradigm, from conventional far-field transmission to near-field communication, where spherical wave propagation becomes dominant. In the near-field region, the channel response, characterized by spherical wavefronts, depends not only on the angles but also on the propagation distance. This additional distance-dependent degree of freedom significantly increases the dimensionality of the channel parameters. As a result, directly applying conventional far-field channel estimation methods, which are designed based solely on angular information, to near-field scenarios often leads to significantly higher pilot overhead and computational complexity. These challenges highlight the urgent need for channel estimation techniques specifically tailored to the unique characteristics of near-field propagation. This paper provides a comprehensive overview of recent advances in near-field channel estimation. From the perspective of electromagnetic wave characteristics, it first defines the boundary between near- and far-field regions and analyzes the fundamental differences in their propagation behaviors, along with a brief review of ELAA-related developments. It then introduces mainstream near-field channel models and contrasts them with their far-field counterparts. Subsequently, it systematically reviews major estimation techniques under various system configurations, including single- and multi-user, as well as single- and multi-carrier systems, covering both direct channel estimation between the base station and user equipments, and cascaded channel estimation assisted by reconfigurable intelligent surface. These techniques reflect different trade-offs among estimation accuracy, algorithmic complexity,

and system overhead. This survey aims to provide technical insights and theoretical foundations for the development of efficient and scalable near-field channel estimation solutions for 6G systems, while also identifying key challenges and potential future research directions.

Index Terms—Near-field wireless communications, spherical wave, near-field channel modeling, near-field channel estimation, extremely large aperture arrays.

I. INTRODUCTION

With the global commercialization and deployment of fifth-generation (5G) wireless communication systems, both academia and industry are actively paving the way for the development of sixth-generation (6G) networks [1]. The aim is to meet the requirements of emerging applications such as the intelligent industrial systems, metaverse, and fully autonomous vehicles [2]–[4]. In June 2023, the International Telecommunication Union (ITU) released its official vision for 6G networks [5], outlining a recommended system architecture, key enabling technologies, and a comprehensive development roadmap. This publication marked the formal initiation of 6G standardization efforts. Notably, the ITU also identifies six representative usage scenarios for 6G systems. These include enhancements to existing 5G paradigms, namely: enhanced mobile broadband (eMBB+), massive machine-type communications (mMTC+), and ultra-reliable low-latency communications (URLLC+); as well as three transformative new use cases: integrated sensing and communication (ISAC), integrated artificial intelligence (AI) and communication, and ubiquitous connectivity. To support these advanced use cases, 6G systems are expected to achieve peak data rates of at least 1 Tb/s, air interface latency as low as 0.01 - 0.1 ms, and device densities up to 10^7 devices/km² [6], [7]. These ambitious performance targets exceed the capabilities of current 5G technologies, necessitating the development of novel and potentially disruptive communication paradigms.

In 6G wireless communications, extremely large aperture arrays (ELAAs) [8], [9] and high-frequency technologies [10], [11] are widely recognized as two key enabling technologies. As a natural evolution of massive multiple-input multiple-output (MIMO) in 5G systems, ELAAs integrate hundreds or even thousands of antenna elements [8], [12], significantly enhancing spatial multiplexing and beamforming capabilities. This leads to substantial improvements in spectral efficiency (SE) and spatial resolution for 6G networks. On the other

W.-X. Long and M. Morelli are with the Dipartimento di Ingegneria dell'Informazione, University of Pisa, 56126 Pisa, Italy (e-mail: wenxuan.long@ing.unipi.it, michele.morelli@unipi.it).

S. Ye and R. Chen are with the State Key Laboratory of Integrated Service Networks, Xidian University, Xi'an 710071, Shaanxi, China (e-mail: 24011211130@stu.xidian.edu.cn, rchen@xidian.edu.cn).

M. Moretti and L. Sanguinetti are with the Dipartimento di Ingegneria dell'Informazione, University of Pisa, 56126 Pisa, Italy, and also with National Inter-University Consortium for Telecommunications (CNIT), 43124 Parma, Italy (e-mail: marco.moretti@unipi.it, luca.sanguinetti@unipi.it).

C.-X. Wang is with the National Mobile Communications Research Laboratory, School of Information Science and Engineering, Southeast University, Nanjing, 211189, China, and also with the Purple Mountain Laboratories, Nanjing 211111, China. (e-mail: chxwang@seu.edu.cn).

This work has been performed in the framework of the HORIZON-JU-SNS-2022 project TIMES, cofunded by the European Union, and also supported in part by Italian Ministry of Education and Research (MUR) in the Framework of the FoReLab Project (Departments of Excellence) and the Project GARDEN funded by EU in NextGenerationEU Plan through Italian "Bando Prin 2022-D.D.1409 del 14-09-2022".

hand, extremely large reconfigurable intelligent surfaces (XL-RISs) [6], [13], typically constructed from metamaterials, can be viewed as a special class of ELAAs consisting of a huge number of passive reflecting elements. By intelligently controlling incident electromagnetic waves, XL-RISs can dynamically reconfigure the wireless propagation environment, offering new opportunities to boost network capacity and coverage. Moreover, the terahertz (THz) band (0.1 - 10 THz) is considered a promising frequency spectrum for 6G systems due to its abundant bandwidth resources [10], [14]. Compared to the millimeter-wave (mmWave) band used in 5G networks (30 - 300 GHz), the THz band offers significantly wider bandwidth, on the order of tens of gigahertz (GHz), making it well suited for supporting the ultra-high data rates envisioned in future 6G systems. It is worth emphasizing that ELAAs and THz technologies exhibit a natural synergy in 6G networks. The sub-millimeter wavelengths used in THz communications allow for dense integration of antenna elements within the compact footprint of a base station (BS), enabling the practical deployment of ELAAs. In turn, the significant array gain offered by ELAAs can effectively mitigate the severe path loss of THz communications. This complementary relationship makes their integration a key enabler for high-performance 6G wireless communications.

More importantly, deploying ELAAs in high-frequency bands not only entails increased carrier frequencies and the number of antenna elements, but also signifies a fundamental shift in the wireless communication paradigm, i.e., from conventional far-field transmission to near-field transmission. The boundary between these two regions is typically defined by the Rayleigh distance [3], which is proportional to the square of the array aperture and inversely proportional to the carrier wavelength. For instance, an array operating at 0.1 THz with a physical aperture of $0.5 \text{ m} \times 0.5 \text{ m}$ yields a Rayleigh distance of approximately 333 m, which essentially covers the entire area of a typical cell. As a result, near-field wireless communication [2], [4], [15]–[17] is anticipated to become a standard operating mode in 6G networks as ELAAs are widely deployed. To accurately capture the channel characteristics in near-field communication, it is essential to adopt a more precise spherical wave propagation model [2], [4], which fundamentally differs from the uniform planar wave approximation widely used in conventional far-field communication systems.

Near-field communications offer compelling advantages, such as the ability to simultaneously exploit spatial degrees of freedom in both the angular and distance domains. This dual-domain control enables fine-grained beam focusing and interference suppression, significantly enhancing spatial resolution and user capacity for 6G systems. These benefits make near-field communications particularly attractive for scenarios such as high-density user access and ISAC systems, where precise spatial discrimination is critical. Despite these benefits, fully harnessing the potential of near-field communications entails notable technical challenges. Due to the inherent spherical wavefront of near-field propagation, the channel response depends on the three-dimensional (3-D) position of the receiver rather than solely on the direction of

arrival (DoA), as in far-field models. Consequently, angular-only channel representations become inadequate, necessitating refined models that jointly account for both angular and distance characteristics [18]. Existing near-field channel modeling efforts are generally classified into three categories: The first category consists of geometry-based spherical wavefront models [19], which characterize near-field channels based on the array geometry of ELAAs and the relative positions of the transceiver pair. These models emphasize the spherical wavefront characteristic inherent to near-field propagation but typically overlook other physical properties such as vector wave field and the multiple polarizations. In line-of-sight (LoS) scenarios, such models typically characterize the channel response as an explicit function of the distance between the transmitter and receiver. The second category, multipath spherical wavefront models [20], is specifically designed for scenarios involving a finite number of propagation paths. Within this framework, the near-field channel is represented as a superposition of multiple spherical wave components, each corresponding to an individual path characterized by different propagation distances and DoAs. The third category comprises spatial correlation models [21], [22], which characterize non-line-of-sight (NLoS) channels using second-order statistics, typically represented by spatial correlation matrices. These models describe a class of NLoS channels with common statistical properties, from which individual channel realizations can be randomly generated. The correlation matrices are generally derived under the assumption of spherical wavefront propagation. These modeling approaches not only capture the unique characteristics of near-field propagation from different perspectives, but also provide essential foundations for downstream signal processing tasks such as channel estimation and beamforming.

Furthermore, as the dimensionality of channel parameters increases, both the pilot overhead and computational complexity required for near-field channel estimation rise significantly. Traditional far-field channel estimation methods, such as least squares (LS) and linear minimum mean square error (LMMSE), are computationally intensive and thus impractical for near-field scenarios. This highlights the need for low-complexity, low-overhead algorithms that leverage the unique structure of spherical wavefronts in near-field propagation. When the near-field channel can be accurately characterized by a limited set of physical parameters, such as the relative distance and DoA between the transmitter and receiver in a LoS scenario, it is possible to reconstruct the channel by estimating these parameters. This leads to the development of parametric channel estimation techniques. In addition, due to the inherent sparsity of near-field channels in the polar domain, sparsity-aware methods have also been widely adopted to jointly recover angular and distance information, enabling accurate reconstruction of the complete near-field channel. Moreover, deep learning approaches show strong potential for near-field channel estimation, providing an effective means to achieve low-complexity and high-efficiency solutions.

Against this backdrop, this survey provides a comprehensive review and analysis of existing channel estimation techniques tailored for near-field communication scenarios.

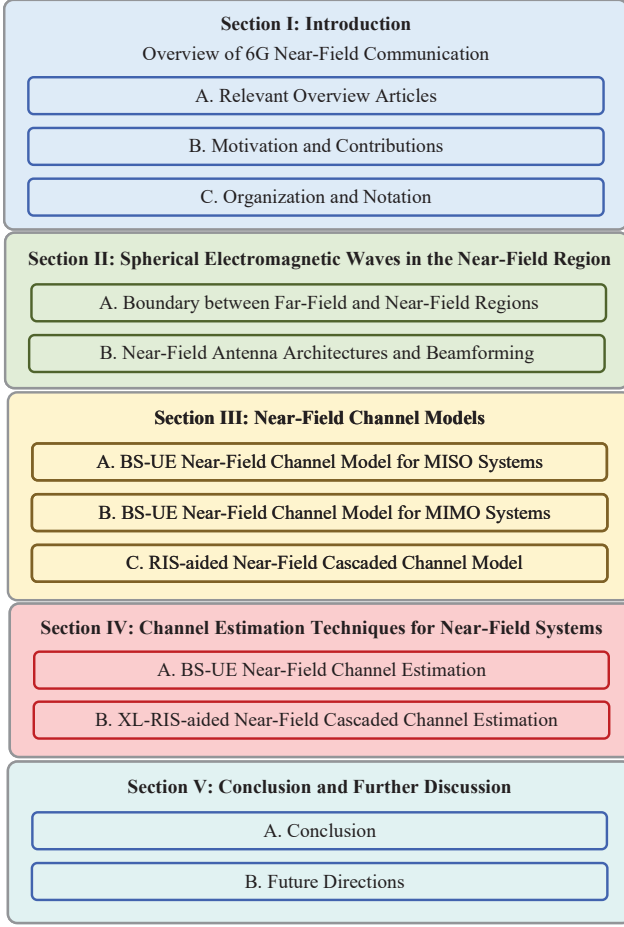


Fig. 1: The structure of this survey.

The discussion covers both direct BS-to-user equipment (UE) channel estimation and RIS-assisted cascaded channel estimation under various deployment configurations. The goal is to consolidate recent advances in near-field channel recovery to ensure the accurate acquisition of channel state information (CSI), thereby laying the foundation for reliable and high-performance near-field communications.

A. Relevant Overview Articles

To date, several surveys [16], tutorials [2], [3], and magazine articles [4], [15], [17], [23] have introduced the fundamental concepts, operating principles, and potential applications of near-field communications, each from a different perspective and with varying levels of depth and focus. Among the earliest efforts, the magazine article [15] provided an introduction to near-field communications, covering the distinction between near- and far-field regions, core concepts, technical challenges, and envisioned applications. It also briefly outlined the idea of channel estimation using near-field-specific codebooks. Following this, the magazine article [17] offered a focused exploration of the fundamental differences between spherical wavefront-based near-field communications and conventional planar wavefront-based far-field communications, particularly in the context of channel modeling, beamforming, system performance, and integration with next-generation technologies. Expanding on this line of

work, the authors of [2] presented a comprehensive tutorial that systematically reviewed near-field channel modeling, antenna architectures, beamforming techniques, and system performance analysis. Building on this tutorial foundation, the same research team extended their investigation in the survey paper [16] by proposing signal processing algorithms tailored to novel array architectures for near-field communications and examining its integration with advanced technologies including RIS and ISAC. Notably, this survey also provides a concise summary of over 20 representative works on near-field channel estimation published prior to 2023. Complementing the above efforts, the magazine article [4] discussed several core technical challenges in near-field communications, spanning channel modeling, estimation, beamforming, hardware design, and sensing, and briefly highlighted recent research efforts in each area. Of particular note, it summarized the limitations faced by codebook-based compressive sensing algorithms in near-field channel estimation and reviewed three representative solutions to address these challenges. From the perspective of extremely large-scale MIMO (XL-MIMO), the tutorial [3] offered a systematic overview of near-field modeling, system performance, and practical design considerations, offering meaningful guidance to researchers working on near-field propagation, especially in relation to array design. Lastly, the magazine article [23] offered an introductory perspective on the challenges posed by spherical wave propagation in the context of user localization and channel estimation, and outlined a few representative algorithmic strategies designed to mitigate these issues. Despite these valuable contributions, a dedicated, systematic, and in-depth survey focusing specifically on near-field channel estimation remains lacking in the literature.

B. Motivation and Contributions

As previously mentioned, near-field communications are envisioned to play a critical role in 6G systems. Ensuring reliable and high-performance near-field transmission necessitates accurate CSI. Despite growing interest, the existing literature lacks a comprehensive and systematic survey on recent advances in near-field channel estimation. This gap serves as the primary motivation for this work. The main contributions of this survey are summarized as follows:

- We begin by discussing the boundary criteria between the far-field, radiative near-field, and reactive near-field regions for different array configurations, defined by the Rayleigh and Fresnel distances. This provides the theoretical foundation for subsequent analysis of near-field communication characteristics. Building upon this, we further present a brief survey of existing ELAAs capable of generating extended near-field regions, including continuous aperture (CAP) arrays and spatially discrete (SPD) arrays, along with their corresponding beamforming and control techniques.
- We discuss representative near-field channel modeling approaches, covering near-field array response vectors for different array configurations, near-field LoS and multipath channel models, as well as spatially correlated

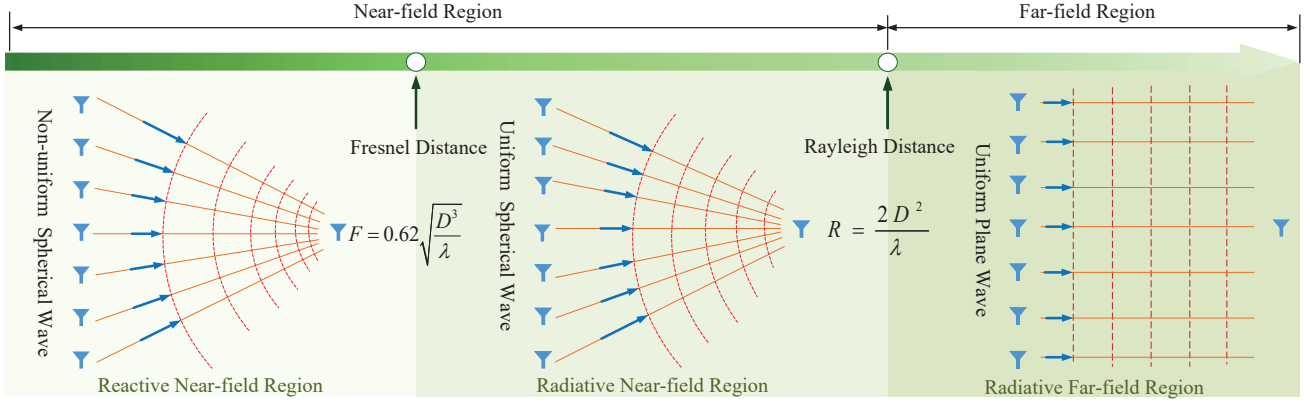


Fig. 2: Field region division for the array antenna

channel models that incorporate near-field characteristics. Subsequently, we provide a comparison with conventional far-field channel models to highlight the fundamental differences in their channel characteristics.

- As the core part of this survey, we provide a systematic summary of recent advances in near-field channel estimation under various system configurations, including single-user and multi-user systems, as well as single-carrier and multi-carrier transmission scenarios. The review covers not only the direct channel estimations between the BS and UEs, but also the cascaded channel estimation techniques in the presence of RIS. For these different types of channel structures, we categorize the main estimation approaches proposed in the literatures, including parametric estimation methods, sparsity-aware techniques, and deep learning-based solutions. These methods exhibit different trade-offs among estimation accuracy, algorithmic complexity, and pilot overhead. This part aims to offer a comprehensive reference and technical roadmap for researchers and engineers working in the field of near-field communications.

C. Organization and Notation

The remainder of this survey is illustrated in Fig. 1. Section II first reviews the boundary between the far-field and near-field regions, and summarizes the mainstream antenna architectures capable of generating spherical waves, along with corresponding wavefront manipulation techniques. Section III presents the fundamental models for near-field channels. Section IV provides a comprehensive overview of existing research on near-field channel estimation across various scenarios. Finally, Section V concludes the survey.

Throughout this paper, scalars are denoted by italic letters (i.e., x), vectors by bold lowercase letters (i.e., \mathbf{x}), and matrices by bold uppercase letters (i.e., \mathbf{X}). The operators $(\cdot)^T$ and $(\cdot)^H$ denote the transpose and Hermitian transpose, respectively. The Euclidean norm of a vector \mathbf{x} is written as $\|\mathbf{x}\|$, while $\mathbb{E}\{\cdot\}$ denotes the expectation operator. The notation $\text{diag}(\mathbf{x})$ refers to a diagonal matrix formed by placing the elements of \mathbf{x} along the main diagonal. Moreover, $\text{mod}(\cdot, \cdot)$ represents the modulo operation, and $\lfloor \cdot \rfloor$ denotes the floor function.

II. SPHERICAL ELECTROMAGNETIC WAVES IN THE NEAR-FIELD REGION

This section begins with a review of existing studies on the boundaries between near-field and far-field regions, followed by an investigation into the generation and control mechanisms of spherical electromagnetic waves within the near-field region.

A. Boundary between Far-Field and Near-Field Regions

As illustrated in Fig. 2, the electromagnetic environment around an antenna array can be divided into the near-field and far-field regions, with the Rayleigh distance marking the boundary between them. The near-field region can be further divided into two subregions: the reactive near-field and the radiative near-field, separated by the Fresnel distance. When the source is located closer to the array than the Fresnel distance, the electromagnetic waves exhibit a strongly non-uniform, spherical wavefront. As the distance increases beyond the Fresnel region, the wavefront becomes more uniform, although it retains some curvature, resulting in a quasi-uniform spherical shape. Eventually, in the far-field region, the electromagnetic radiation degenerates into a uniform plane wave.

1) *Rayleigh Distance*: The Rayleigh distance serves as the boundary between the far-field and radiative near-field regions of an antenna array. Within the Rayleigh distance, due to variations in the propagation path lengths, the angular field distribution is dependent on the position of the receiver, resulting in a spherical wavefront. Beyond this distance, the propagation paths from individual points on the transmitter to the receiver can be approximated as mutually parallel. As a result, the angular field distribution becomes independent of the receiver location, and the wavefront can be considered planar. The expression for the Rayleigh distance is given by

$$R = \frac{2D^2}{\lambda}, \quad (1)$$

where D and λ is the maximum aperture of the array and the wavelength, respectively. From (1), the Rayleigh distance is proportional to the square of the array size and inversely proportional to the carrier wavelength. When the distance between the array and the source exceeds R , the planar wavefront assumption holds. Otherwise, the phase variation

TABLE I: Rayleigh distance and Fresnel distance of different arrays

Boundary	Ref.	Communication system	Inter-element spacing	Array			Distance formula
				ULA	UPA	UCA	
Rayleigh distance	[33]	–	–	–	–	–	$2D^2/\lambda$
	[20], [24], [25], [26]	MISO	Half-wavelength	✓			$N^2\lambda/2$
	[27]	MIMO	Half-wavelength	✓			$\lambda(N_t + N_r)^2/2$
	[34], [28], [13]	MISO	d_t		✓		$2d_t^2(N_H^2 + N_V^2)/\lambda$
	[29], [30]	MISO	Half-wavelength		✓		$(N_H^2 + N_V^2)\lambda/2$
	[31], [32]	MISO	d_t			✓	$8r_{UCA}^2/\lambda$
Fresnel distance	[35]	–	–	–	–	–	$0.62\sqrt{D^3/\lambda}$
	[36]	MISO	d_t	✓			$0.62\sqrt{(Nd_t)^3/\lambda}$
	[34], [28]	MISO	d_t		✓		$0.62\sqrt{d_t^3(N_H^2 + N_V^2)^{3/2}/\lambda}$
	[34]	MISO	d_t			✓	$0.62\sqrt{8r_{UCA}^3/\lambda}$

across the array elements is no longer linear with respect to their position, and a spherical wave propagation model must be adopted.

According to [20], [24]–[26], for a multiple-input single-output (MISO) system equipped with a uniform linear array (ULA) and an inter-element spacing of $d_t = \lambda/2$, the array aperture D can be expressed as $D = Nd_t = N\lambda/2$, where N denotes the number of ULA elements. Accordingly, the Rayleigh distance for the ULA-based MISO system is calculated as

$$R_{ULA}^{MISO} = \frac{1}{2}N^2\lambda. \quad (2)$$

For a ULA-based MIMO system with N_t transmit and N_r receive elements, and an inter-element spacing of $d_t = d_r = \lambda/2$, the Rayleigh distance is given by [27]

$$R_{ULA}^{MIMO} = \frac{\lambda(N_t + N_r)^2}{2}. \quad (3)$$

As stated in [28], the Rayleigh distance for a MISO system equipped with a uniform planar array (UPA), characterized by N_H rows and N_V column, and an inter-element spacing of d_t , can be expressed as

$$R_{UPA}^{MISO} = \frac{2d_t^2(N_H^2 + N_V^2)}{\lambda}. \quad (4)$$

When the inter-element spacing $d_t = \lambda/2$, equation (4) can be further simplified as [13], [29], [30]:

$$\bar{R}_{UPA}^{MISO} = \frac{(N_H^2 + N_V^2)\lambda}{2}. \quad (5)$$

Finally, for a MISO system employing a uniform circular array (UCA) with radius r_{UCA} , the Rayleigh distance is expressed in [31], [32] as

$$\bar{R}_{UCA}^{MISO} = \frac{8r_{UCA}^2}{\lambda}. \quad (6)$$

For the sake of convenience, the Rayleigh distances for different array types are summarized in Table I.

2) *Fresnel Distance*: The Fresnel distance further divides the near-field region into reactive and radiative subregions. When the distance between the array and a point source is below this threshold, the electric and magnetic fields become not in phase, resulting in localized oscillation of electromagnetic energy rather than effective radiation. As a result, the electromagnetic wave exhibits a highly non-uniform spherical wavefront. Due to their rapid spatial attenuation, such waves are confined to a very limited region near the antenna. Beyond the Fresnel distance, the wavefront becomes progressively regular and can be approximated as a uniform spherical wave. Originally introduced by C. Polk in [37], the general expression for the Fresnel distance is given by

$$F = 0.62\sqrt{\frac{D^3}{\lambda}}. \quad (7)$$

According to (7), the Fresnel distance increases with a larger array size D and with a shorter wavelength λ . For a MISO system employing a ULA, the Fresnel distance can be expressed as [36]

$$F_{ULA}^{MISO} = 0.62\sqrt{\frac{(Nd_t)^3}{\lambda}} \quad (8)$$

while in the case of a UPA-based MISO system, where the array aperture is given by $D = d_t\sqrt{(N_H^2 + N_V^2)}$, we have

$$F_{UPA}^{MISO} = 0.62\sqrt{\frac{d_t^3(N_H^2 + N_V^2)^{3/2}}{\lambda}}. \quad (9)$$

Finally, for a MISO system utilizing a UCA with radius r_{UCA} , the Fresnel distance is given by

$$F_{UCA}^{MISO} = 0.62\sqrt{\frac{8r_{UCA}^3}{\lambda}}. \quad (10)$$

TABLE II: Comparison of characteristics of different ELAA architectures

Type	Structure		Transmission Mode	Power Budget	Element Density	Control Type	Main Functions
CAP Array	DMA		Active	Medium	Dense or extremely dense	Dynamic amplitude /phase control	BS and Mobile terminals
	Continuous HMIMO		Active	Medium-High	Near-continuous	Continuous holographic control	Future XL-MIMO systems
	RIS		Passive or quasi-passive	Low	Dense or extremely dense	Dynamic phase control	Assisted communications
	LIS		Active or quasi-passive	Medium-High	Continuous	Continuous surface control	Future indoor/macro coverage
SPD Array	Massive MIMO		Active	Medium-High	Sparse	Hybrid beamforming	5G BS
	XL-MIMO		Active	High	Sprase or relatively dense		B5G/6G BS
	Discrete HMIMO	Discrete RIS	Passive or quasi-passive	Low	Relatively dense or quasi-continuous	Dynamic phase control	Assisted communications
		Discrete LIS	Active or quasi-passive	Medium-High	Relatively dense or quasi-continuous	Dynamic amplitude/phase control	Future indoor/macro coverage

For easier comparison, the analytical expressions for the Fresnel distance across different array configurations are summarized in Table I.

B. Near-Field Antenna Architectures and Beamforming

With the continuous growth in wireless communication demands, the massive MIMO in 5G networks is evolving toward the ELAAs to meet the requirements of Beyond 5G (B5G) networks for higher capacity and data rates. Generally, based on the ratio between the antenna element size A and the square of the inter-element spacing d :

$$\xi \triangleq \frac{A}{d^2}, \quad (11)$$

ELAAs can be classified into CAP arrays and SPD arrays [38]. In the extreme case when $\xi = 1$, the discrete array will transform into a continuous holographic surface. According to (1), the deployment of ELAAs leads to a significant increase in array aperture, which substantially extends the near-field region and positions near-field communication as a potential cornerstone for 6G wireless systems. Moreover, it is noteworthy that the Fresnel distance of SPD arrays is typically negligible in practical communication scenarios, as non-uniform propagation is confined to a very limited region around each antenna element. In contrast, CAP arrays, owing to their large continuous radiating surface, generally exhibit a non-negligible Fresnel distance [17]. In the following, we provide a brief review of existing CAP and SPD array structures applicable to near-field communications, along with their corresponding near-field beamforming techniques.

1) *Continuous-Aperture Array*: Generally speaking, a CAP array is composed of a large number of elements with infinitesimal spacing between them [16]. Due to the significant challenges associated with deploying a large number of antenna elements within a finite array aperture, CAP arrays are typically realized using emerging metamaterial technologies [39]. Existing metamaterial-based antennas mainly include dynamic metasurface antennas (DMAs) [40]–[43], the RISs [44]–[47], the continuous holographic MIMO (HMIMO) [48]–[51] and the large intelligent surfaces (LISs).

Specifically, the DMA is a planar architecture consisting of numerous sub-wavelength elements whose electromagnetic

responses, such as amplitude and phase, can be dynamically and electronically controlled. Unlike traditional phased arrays, DMAs integrate radio-frequency (RF) analog combining directly within the antenna structure, enabling low-complexity, low-cost, and energy-efficient beamforming and spatial multiplexing. The authors of [40] designed a DMA-based transceiver architecture operating at 5.39 GHz for a spatial multiplexing system, leveraging the tunability of DMA elements to enhance system capacity. In [41], [42], the DMA-based massive MIMO arrays were equipped at the BS, effectively reducing power consumption and hardware costs, two major bottlenecks in conventional massive MIMO systems. [43] introduced an advanced antenna architecture in which a DMA, consisting of multiple independently fed waveguide elements, was employed to generate holographic electromagnetic waveforms, thereby further demonstrating the versatility and wavefront control capabilities of DMAs.

Moreover, the RIS is a planar metasurface composed of a large number of passive reflecting elements, each capable of independently adjusting the phase or other characteristics of incident electromagnetic waves, thereby reshaping the wireless propagation environment without active RF transmission or reception. [45] designed a RIS with 256 elements, utilizing positive intrinsic-negative (PIN) diodes within the metamaterials to achieve 2-bit phase shifting, thereby demonstrating the feasibility and efficiency of RIS in MIMO systems. In addition to PIN diodes, [46] also demonstrated the feasibility of deploying RIS using the complementary metal-oxide-semiconductor (CMOS) technology.

Additionally, continuous HMIMO utilizes densely packed or nearly continuous antenna elements distributed across a surface to generate, manipulate, and detect electromagnetic wavefronts based on holographic principles, in order to achieve extremely fine-grained beamforming and ultra-high spatial multiplexing. [48] depicted an 8×8 HMIMO antenna embedded in a $12 \text{ cm} \times 12 \text{ cm}$ square substrate, with inter-element spacing significantly less than half a wavelength, achieving ideal array gain with a small-sized array and demonstrating the potential of metasurface antennas in beam steering. The authors of [49], [50] presented a dynamically reconfigurable HMIMO composed of a set of super-wavelength slot-shaped metamaterial elements for sampling guided modes, where the

coupling response of the metamaterial elements is electronically controlled using of PIN diodes.

Furthermore, the LIS consists of large surfaces embedded within the environment, such as walls and ceilings, that are electromagnetically activated to actively or passively transmit, receive, reflect, or modulate electromagnetic signals. Acting as massive distributed antenna arrays, these electrically active surfaces can significantly enhance wireless communication capacity, coverage, and reliability. [52] presented an implementation of LIS using liquidcrystal-loaded metasurface. In [53], a 3-D LIS with a spherical configuration is proposed for positioning applications. Finally, the different CAP arrays are summarized in Table II for ease of comparison.

Benefiting from its continuity property, the CAP array can generally achieve smoother beamforming, making them well suited for a broader frequency range and for the realization of more complex beam shapes. Consequently, CAP arrays are expected to provide improved directionality and a large gain in near-field communications. However, because of their complex structure, beamforming with CAP arrays typically requires significant signal processing. The authors of [19] proposed a beam focusing scheme aimed at maximizing the achievable sum rate in multi-user near-field communications based on DMA. Additionally, a joint active and passive beamforming scheme is presented in [54] and [55] for RIS-aided MIMO communications, which optimizes both the transmit precoding vector at the BS and the phase-shift parameters at the RIS in order to maximize the total received signal power or minimize the signal-to-interference-plus-noise ratio (SINR) for users. In [56], a hybrid beamforming scheme is designed for RIS-aided MIMO communications, implementing digital beamforming at the BS and analog beamforming at the RIS to achieve sum-rate maximization. In [57], a near-field reception beamforming method is proposed for continuous HMIMO-based uplink transmissions to cope with performance degradations caused by near-field propagation, frequency selectivity, and spatial wideband effects in wideband applications. Compared to conventional hybrid analog and digital combiners, this solution achieves a higher overall transmission rate. In [58], the authors proposed a passive beamforming method aimed at maximizing the received signal-to-noise ratio (SNR) in a passive beamforming and information transfer (PBIT)-enhanced single-input multiple-output (SIMO) system with LIS. The beamforming design was formulated as an optimization problem and solved using the semidefinite relaxation (SDR) technique.

2) *Spatially-Discrete Array*: Compared to CAP arrays, SPD arrays are typically composed of a limited number of antenna elements with fixed inter-element spacing, which results in a discrete aperture. SPD arrays have been widely adopted in existing wireless communications, such as in the MIMO systems used in 4G networks and the massive MIMO systems deployed in 5G networks. The authors of [59], [60] proposed a massive hybrid MIMO array architecture for mmWave cellular communications, where antenna elements are organized into analog subarrays that transmit or receive single digital signals through connected phase shifters, effectively enhancing multiplexing gains. Furthermore, with the explosive growth of

wireless communication demands, SPD arrays are evolving from the massive MIMO systems in current 5G networks toward XL-MIMO systems envisioned for B5G networks. In [61], a total of 3,200 low-cost antenna elements were deployed over a 6-square-meter surface to construct a XL-MIMO array called RFocus, which significantly improves both the median signal strength and the channel capacity.

Additionally, by deploying a large number of antenna elements with sub-wavelength spacing within a compact area, SPD arrays can closely approximate CAP arrays. This configuration leads to the emergence of quasi-continuous aperture antennas, also known as discrete HMIMO [62], which typically includes discrete RIS and discrete LIS. In [63], a discrete RIS consisting of 1,600 elements was designed, where reconfigurable phase control for single polarization is achieved by integrating a PIN diode into each element. The authors of [64] designed an 8×8 space-time coding RIS relying on time modulation of the reflection coefficient. In [65], a dynamically reconfigurable metasurface is developed that is optically driven by integrating photodiodes into the array elements. By illuminating the photodiodes to generate optical signals, the voltage of varactors can be dynamically adjusted, thereby enabling programmable electromagnetic functionality. Besides, the authors of [66] designed a discrete LIS, in which 1,024 elements with half-wavelength spacing in the 4 GHz band are integrated into a $1.2 \text{ m} \times 1.2 \text{ m}$ surface area. Similarly, different SPD arrays are summarized in Table II to facilitate intuitive comparison.

Owing to the deployment of a large number of antenna elements, SPD arrays are capable of flexibly steering signal energy to specific locations through effective near-field beamforming based on environmental changes and user demands. Considering that fully digital beamforming in practical applications suffers from high power consumption, elevated costs, and increased system complexity, existing SPD arrays, such as massive MIMO and XL-MIMO, predominantly adopt hybrid beamforming architectures to generate near-field beams [67]. For the massive MIMO system, the authors of [68] compared the performance of different beamforming schemes, including the maximum ratio transmission (MRT), zero-forcing (ZF), minimum mean square error (MMSE), and signal-to-leakage-noise ratio (SLNR), in the context of millimeter-wave near-field communication. Their investigation shows that, among the solutions considered, the SLNR scheme exhibits the best performance. For XL-MIMO systems, the authors of [69] exploited the spatial structural characteristics of mmWaves to design a beamforming scheme based on the orthogonal matching pursuit (OMP) algorithm, achieving near-optimal hybrid precoding performance. In addition to the OMP-based methods, manifold optimization techniques based on the alternating minimization algorithm [70], [71] can also achieve near-optimal precoding performance. In [72], a two-stage hybrid beamforming structure was employed at both the transmitter and receiver to reduce the number of RF chains and maximize the SE of XL-MIMO systems. The authors of [26] developed a hybrid beamforming structure that incorporates a phase-delay focusing (PDF) method to tackle the near-field beam split issue in XL-MIMO systems. Additionally,

[73] proposed a dynamic hybrid beamforming architecture for near-field XL-MIMO systems, which employs a switching module designed to maximize the sum rate, while minimizing hardware power consumption.

For discrete RIS-aided MIMO systems, [74] developed a deep learning-based end-to-end optimization framework for near-field wideband beamforming, aiming to maximize SE while mitigating the double beam split effect. Besides, a three-dimensional (3-D) beamforming scheme for discrete LIS-aided near-field communication was proposed in [29], consisting of two steps. The first step applies conventional two-dimensional (2-D) far-field beamforming to compensate for phase variations induced by azimuth and elevation angles. The second step performs one-dimensional (1-D) near-field beamforming to correct residual phase variations caused by distance differences.

III. NEAR-FIELD CHANNEL MODELS

When an ELAA is deployed at the BS, its array aperture may reach several tens or even hundreds of wavelengths. As a result, the extension of the Rayleigh distance makes it highly likely that UEs will be located within the near-field region of the BS. As an example, consider a BS array with a physical size of $0.2 \times 0.1 \text{ m}^2$ and inter-element spacing $d = 2\lambda$, operating at 0.3 THz (corresponding to $\lambda = 1 \text{ mm}$). This configuration yields a total of $N = 5000$ antennas arranged in a 100×50 layout. For this array, the Rayleigh distance is $R = 100 \text{ m}$, which spans a substantial portion of a typical cell. As a result, it is highly likely that the UEs operate within the radiative near-field of the BS.

Owing to the large aperture of ELAAs, the propagation distances and angles between individual antenna elements and the UE or scatterers can vary significantly when these objects reside within the array's near-field region. Such variations lead to pronounced amplitude and phase fluctuations across the array, posing considerable challenges for accurate near-field channel modeling. To this end, this section introduces a representative channel modeling framework grounded in the spherical wavefront assumption.

A. BS-UE Near-Field Channel Model for MISO Systems

We begin by considering a MISO system where the UE is equipped with a single antenna and the BS employs an antenna array with N elements. The array response vector at the BS is given by:

$$\mathbf{a}(\theta, \phi, r) = \frac{1}{\sqrt{N}} \left[1, \dots, e^{-j\frac{2\pi}{\lambda}(r_n - r)}, \dots, e^{-j\frac{2\pi}{\lambda}(r_N - r)} \right]^T, \quad (12)$$

where r denotes the distance from the UE to the BS reference element, θ and ϕ are the elevation and azimuth angles of the UE with respect to this element, while r_n is the distance from the n -th BS array element to the UE. Denoting by $\mathbf{u}_n =$

$[x_n, y_n, z_n]^T$ the coordinates of the n -th BS element relative to the reference element, we have

$$\begin{aligned} r_n &= \|\mathbf{r} - \mathbf{u}_n\| \\ &= r \sqrt{1 - \frac{2\mathbf{k}^T(\theta, \phi) \mathbf{u}_n}{r} + \frac{\|\mathbf{u}_n\|^2}{r^2}} \\ &\stackrel{(a)}{=} r - \mathbf{k}^T(\theta, \phi) \mathbf{u}_n + \frac{\|\mathbf{u}_n\|^2 - (\mathbf{k}^T(\theta, \phi) \mathbf{u}_n)^2}{2r} \\ &\quad + \frac{\mathbf{k}^T(\theta, \phi) \mathbf{u}_n \|\mathbf{u}_n\|^2}{2r^2} - \frac{\|\mathbf{u}_n\|^4}{8r^3} + \dots, \end{aligned} \quad (13)$$

where $\mathbf{k}(\theta, \phi) = [\cos \theta \cos \phi, \cos \theta \sin \phi, \sin \theta]^T$ denotes the propagation direction vector from the UE to the BS, and (a) utilizes the Taylor series expansion $\sqrt{1+x} = 1 + \frac{1}{2}x - \frac{1}{8}x^2 + \dots$. Then, the distance difference in (12) can be expressed as:

$$\begin{aligned} \Delta r_n &= r_n - r \stackrel{(b)}{=} -\mathbf{k}^T(\theta, \phi) \mathbf{u}_n + \frac{\|\mathbf{u}_n\|^2 - (\mathbf{k}^T(\theta, \phi) \mathbf{u}_n)^2}{2r} \\ &\quad + \frac{\mathbf{k}^T(\theta, \phi) \mathbf{u}_n \|\mathbf{u}_n\|^2}{2r^2} - \frac{\|\mathbf{u}_n\|^4}{8r^3} + \dots \end{aligned} \quad (14)$$

When the distance r between the BS and the UE exceeds the Rayleigh distance, the Taylor approximation $\sqrt{1+x} \approx 1 + \frac{1}{2}x$ under the far-field condition is applied, where only the first term in (14) is considered, resulting in

$$\Delta r_n = -\mathbf{k}^T(\theta, \phi) \mathbf{u}_n. \quad (15)$$

Furthermore, when the distance r lies between the Rayleigh distance and the Fresnel distance, the following Fresnel approximation can be obtained:

$$\Delta r_n = -\mathbf{k}^T(\theta, \phi) \mathbf{u}_n + \frac{\|\mathbf{u}_n\|^2 - (\mathbf{k}^T(\theta, \phi) \mathbf{u}_n)^2}{2r}. \quad (16)$$

Unlike the far-field approximation in (15), the near-field formulations in (14) and (16) indicate that the array response vector depends not only on the DoA from the UE to the BS, but also on their separation distance.

Under the quasi-static channel assumption, the UE-BS channel with a single LoS path can be modeled as [27]:

$$\mathbf{h}_{\text{NF}}^{\text{LoS}} = g_{\text{NF}}^{\text{LoS}} \mathbf{a}(\theta, \phi, r), \quad (17)$$

where $g_{\text{NF}}^{\text{LoS}}$ is the attenuation factor with zero mean and variance β_{LoS} . On the other hand, when multiple transmission paths are present between the UE and the BS, the multipath channel model can be expressed as [27], [75], [76]:

$$\mathbf{h}_{\text{NF}}^{\text{mul}} = \sqrt{\frac{N}{L}} \sum_{l=1}^L g_l \mathbf{a}(\theta_l, \phi_l, r_l), \quad (18)$$

where g_l is the attenuation factor of the l -th path with zero mean and variance β_{mul} , while (θ_l, ϕ_l, r_l) is the position of the l -th scatterer relative to the reference element of the BS array, $l = 1, \dots, L$. As $L \rightarrow \infty$, we obtain the spatially correlated Rayleigh fading model [28], [77]

$$\mathbf{h}_{\text{NF}}^{\text{Ray}} \sim \mathcal{CN}(\mathbf{0}_N, \mathbf{R}_{\text{Ray}}), \quad (19)$$

where the spatial correlation matrix \mathbf{R}_{Ray} is given by:

$$\mathbf{R}_{\text{Ray}} = \mathbb{E} \{ \mathbf{h} \mathbf{h}^H \} = \beta_{\text{Ray}}.$$

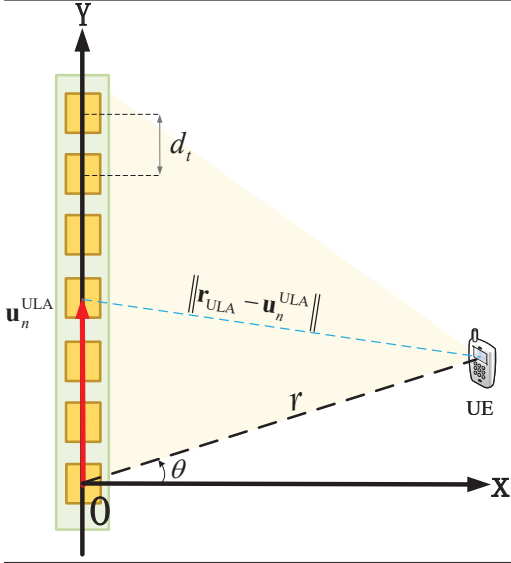


Fig. 3: ULA-based near-field channel model.

$$\int_{r_1}^{r_2} \int_{\varphi_1}^{\varphi_2} \int_{\theta_1}^{\theta_2} f(\tilde{\theta}, \tilde{\phi}, \tilde{r}) \mathbf{a}(\tilde{\theta}, \tilde{\phi}, \tilde{r}) \mathbf{a}^H(\tilde{\theta}, \tilde{\phi}, \tilde{r}) d\tilde{\theta} d\tilde{\phi} d\tilde{r}. \quad (20)$$

In the above equation, β_{Ray} is the average channel power, $\tilde{\theta} \in [\theta_1, \theta_2]$, $\tilde{\phi} \in [\phi_1, \phi_2]$ and $\tilde{r} \in [r_1, r_2]$ define the spatial distribution range of the UE-BS channel, while $f(\tilde{\theta}, \tilde{\phi}, \tilde{r})$ is the normalized spatial scattering function satisfying $\int_{r_1}^{r_2} \int_{\varphi_1}^{\varphi_2} \int_{\theta_1}^{\theta_2} f_h(\tilde{\theta}, \tilde{\phi}, \tilde{r}) = 1$. As an alternative to the Rayleigh fading model, the Rician distribution can be employed to characterize scenarios where both LoS and NLoS paths coexist between the UE and the BS. In such cases, the channel vector is expressed as:

$$\mathbf{h}_{\text{NF}}^{\text{Ric}} \sim \mathcal{CN}(\mathbf{h}_{\text{NF}}^{\text{LoS}}, \mathbf{R}_{\text{Ric}}), \quad (21)$$

where $\mathbf{h}_{\text{NF}}^{\text{LoS}}$ denotes the mean of the Rician model, while the correlation matrix is defined as

$$\mathbf{R}_{\text{Ric}} = \mathbb{E} \left\{ (\mathbf{h}_{\text{NF}}^{\text{Ric}} - \mathbf{h}_{\text{NF}}^{\text{LoS}}) (\mathbf{h}_{\text{NF}}^{\text{Ric}} - \mathbf{h}_{\text{NF}}^{\text{LoS}})^H \right\}. \quad (22)$$

As is seen, when $\mathbf{h}_{\text{NF}}^{\text{LoS}} = \mathbf{0}_N$, i.e., only NLoS paths exist between the UE and the BS, the Rician fading model in (21) reduces to the Rayleigh fading model in (19). The above equations from (17) to (22) indicate that, in the MISO scenario, the array response vector at the BS is the dominant factor in characterizing the UE-BS channel. Hence, in the sequel we provide the array response vectors for various BS array geometries.

1) *ULA-based Channel Model:* We first consider a MISO system where the BS is equipped with a ULA with inter-element spacing d_t . In such a case, we can always consider a coordinate system as shown in Fig. 3, such that all the ULA elements lie within the XOY plane. Under this configuration, the Z-axis can be ignored and we can set $\theta = 0^\circ$. By placing the origin of the coordinate system at the reference element of the ULA, the coordinates of the n -th ULA element are expressed as $\mathbf{u}_n^{\text{ULA}} = [0, nd_t]^T$, where $n = 1, 2, \dots, N$. Furthermore, the coordinates of the UE antenna are given by $\mathbf{r}_{\text{ULA}} = r \mathbf{k}_{\text{ULA}} = r [\cos \phi, \sin \phi]^T$, where r and ϕ denote the distance and azimuth angle between the reference element of

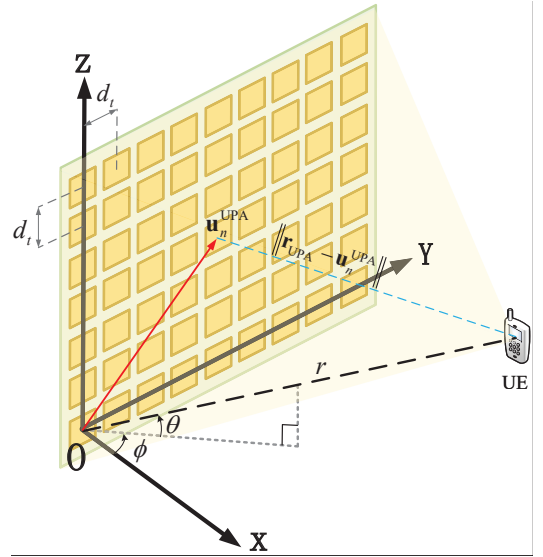


Fig. 4: UPA-based near-field channel model.

the ULA and the UE. In this case, the propagation distance $\|\mathbf{r}_{\text{ULA}} - \mathbf{u}_n^{\text{ULA}}\|$ from the n -th ULA element to the UE can be calculated as [78]:

$$\begin{aligned} \|\mathbf{r}_{\text{ULA}} - \mathbf{u}_n^{\text{ULA}}\| &= \sqrt{r^2 + (nd_t)^2 - 2rnd_t \sin \phi} \\ &= r - nd_t \sin \phi + \frac{(nd_t)^2 \cos^2 \phi}{2r} + \dots \end{aligned} \quad (23)$$

Based on (23), the difference between the path lengths from the UE to the n -th ULA element and from the UE to the ULA reference element is expressed by

$$\begin{aligned} \Delta r_n^{\text{ULA}} &= \|\mathbf{r}_{\text{ULA}} - \mathbf{u}_n^{\text{ULA}}\| - r \\ &= -nd_t \sin \phi + \frac{(nd_t)^2 \cos^2 \phi}{2r} + \dots \end{aligned} \quad (24)$$

Substituting (24) into (12), we obtain the near-field array response vector for the ULA as

$$\mathbf{a}_{\text{ULA}}(\phi, r) = \frac{1}{\sqrt{N}} \left[1, \dots, e^{-j \frac{2\pi}{\lambda} \Delta r_n^{\text{ULA}}}, \dots, e^{-j \frac{2\pi}{\lambda} \Delta r_N^{\text{ULA}}} \right]^T. \quad (25)$$

Finally, putting this array vector into (17), (18), (20), and (22), we can sequentially derive the ULA-based LoS channel model [21], [78], the multipath channel model [21], [78], the spatially correlated Rayleigh model [79], [80], and the Rician channel model [79], [80] in the near-field case.

2) *UPA-based Channel Model:* We now consider a BS equipped with a 2-D UPA with inter-element spacing d_t , where the number of elements in each row and column are denoted by N_H and N_V , respectively. As illustrated in Fig. 4, we employ a 3-D coordinate system at the BS, with the UPA lying on the YOZ plane and the reference element placed in the origin O. When the UPA elements are indexed in a row-by-row manner with $n \in [1, N]$, where $N = N_H \times N_V$, the location of the n -th UPA element is expressed as $\mathbf{u}_n^{\text{UPA}} = [0, i_n d_t, j_n d_t]^T$, where $i_n = \text{mod}(n-1, N_H)$ and $j_n = \lfloor (n-1)/N_H \rfloor$. On the other hand, the coordinates of the UE antenna are given by $\mathbf{r}_{\text{UPA}} = r \mathbf{k}_{\text{UPA}} = r [\cos \theta \cos \phi, \cos \theta \sin \phi, \sin \theta]^T$, where r , θ and ϕ are the distance, elevation and azimuth angles between

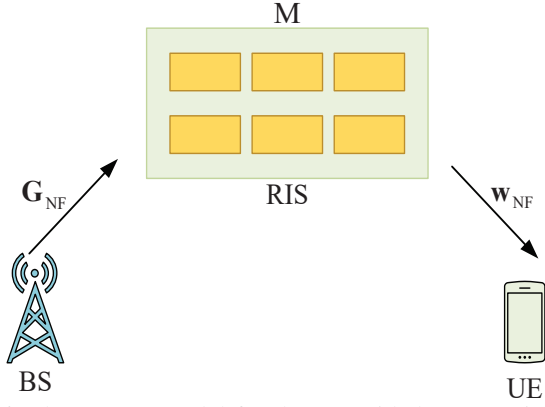


Fig. 6: The system model for the RIS-aided communications.

models in (17)–(22) and (30)–(32) allows for a natural extension to dynamic channel scenarios [93]–[95]. For clarity, we summarize the characteristics of different channels in Table III.

C. RIS-aided Near-Field Cascaded Channel Model

When an obstruction exists between the BS and the UE, a RIS can be employed to reflect the UE signals towards the BS through phase-shift adjustments, as shown in Fig. 6. When the UE is equipped with a single antenna, while the BS and RIS are equipped with N_t and M elements, respectively, the channel model of the RIS-aided system consists of two components: the channel $\mathbf{w}_{\text{NF}} \in \mathbb{C}^M$ from the UE to the RIS, and the channel $\mathbf{G}_{\text{NF}} \in \mathbb{C}^{N_t \times M}$ between the RIS and the BS. Thus, the cascaded channel from the UE to the BS, reflected by the RIS, can be expressed as [25], [96]–[104]

$$\mathbf{x} = \mathbf{G}_{\text{NF}} \mathbf{\Theta} \mathbf{w}_{\text{NF}} = \mathbf{G}_{\text{NF}} \text{diag}(\mathbf{w}_{\text{NF}}) \boldsymbol{\phi} = \mathbf{h}_{\text{cas}} \boldsymbol{\phi}, \quad (33)$$

where $\boldsymbol{\phi} \in \mathbb{C}^M$ is the vector collecting the controllable RIS phase-shifts $\{\phi_m \in [0, 2\pi); m = 1, \dots, M\}$, $\mathbf{\Theta} = \text{diag}(\boldsymbol{\phi})$ and $\mathbf{h}_{\text{cas}} = \mathbf{G}_{\text{NF}} \text{diag}(\mathbf{w}_{\text{NF}})$. When the UE is equipped with N_r elements, the cascaded channel model from the UE to the RIS and then to the BS is given by [105]–[108]

$$\mathbf{X} = \mathbf{G}_{\text{NF}} \mathbf{\Theta} \mathbf{W}_{\text{NF}}, \quad (34)$$

where $\mathbf{W}_{\text{NF}} \in \mathbb{C}^{M \times N_r}$ is the UE-RIS channel. The specific modeling of channels \mathbf{G}_{NF} and \mathbf{w}_{NF} (or \mathbf{W}_{NF}) is derived by taking into account the geometric configuration of the arrays employed at the UE, BS, and RIS, as outlined in Section III-A and Section III-B.

Although both this section and the literature [2], [109] have established preliminary deterministic and statistical modeling frameworks for near-field channels, several critical challenges remain unresolved. The key challenges are summarized as follows [109]:

- **Spatial non-stationarity awareness:** In near-field transmission with ELAAs, spatial non-stationarity is a fundamental characteristic that must be accurately incorporated into channel models [110]. Capturing this property often requires extensive scenario-specific measurement data, thereby motivating the development of non-stationarity-aware channel modeling approaches.
- **Concise channel models with controllable dimensionality:** The introduction of ELAAs can result in near-field channel models with extremely high dimensionality, leading to significant computational overhead and costly parameter estimation. Hence, developing concise models with controllable dimensions is essential. However, achieving a balance between model simplicity and accuracy remains a key challenge.
- **Mutual coupling awareness:** In near-field systems with CAP arrays, mutual coupling between antenna elements is generally non-negligible. The radiated field from each element influences its neighboring elements, and these interactions propagate recursively across the array, altering the overall channel response. Therefore, incorporating mutual coupling into channel models is essential for accurate characterization and effective exploitation of near-field behavior.
- **Vectorial wavefront inclusion:** In addition to spherical wavefronts, vector wavefields are a fundamental characteristic of near-field channels and must be accurately captured in the modeling process. However, most existing models are built on scalar wavefield assumptions, which overlook vectorial effects. Furthermore, near-field

TABLE III: Far-field vs. near-field channel comparison.

System	Channel Model	Characteristic	Main Factors	Type	DoFs	
MISO	Far-field	Linear phase	DoA	LoS	1	
				NLoS	Multipath	1
					Rayleigh	1
				Rician	1	
	Near-field	Non-linear phase	DoA and distance	LoS	1	
				NLoS	Multipath	1
					Rayleigh	1
Rician				1		
MIMO	Far-field	Linear phase	DoA	LoS	1	
				NLoS	Multipath	≥ 1
					Rayleigh	≥ 1
				Rician	≥ 1	
	Near-field	Non-linear phase	DoA and distance	LoS	≥ 1	
				NLoS	Multipath	≥ 1
					Rayleigh	≥ 1
Rician				≥ 1		

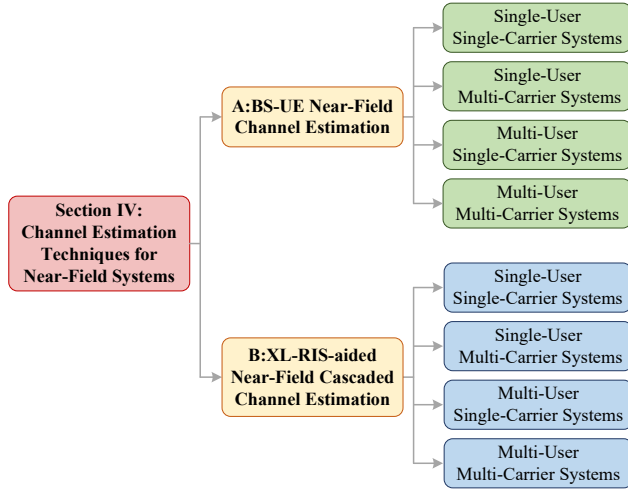


Fig. 7: The classification of near-field channel estimation scenarios in Section IV.

channel models should account for polarization effects.

In summary, addressing the above challenges is of great significance for advancing near-field channel modeling theory and provides a clear roadmap for future research in this area.

IV. CHANNEL ESTIMATION TECHNIQUES FOR NEAR-FIELD SYSTEMS

In the previous section, we introduced near-field channel models for conventional MISO, MIMO, and RIS-aided communication systems. It is worth emphasizing that, compared to far-field channels, the electromagnetic wave characteristics in near-field transmission shift from planar waves to spherical waves, thereby adding an extra distance dimension to the channel model. The inclusion of the distance dimension not only increases the system complexity, but also presents greater challenges for channel estimation. In this section, we will provide a comprehensive overview of existing near-field channel estimation methods. By considering various system configurations as illustrated in Fig. 7, we systematically analyze solutions tailored to single-user, multi-user, single-carrier, and multi-carrier scenarios. These methods aim to balance complexity and performance, offering technical support for the efficient implementation of near-field communication systems.

A. BS-UE Near-Field Channel Estimation

In the near-field scenario, conventional channel estimation schemes based on the LS or LMMSE [28], [126], [127] methods are still applicable. However, with the introduction of the ELAA, the dimensionality of near-field channels increases significantly and, in such a case, conventional channel estimation algorithms would require substantial overhead and high computational complexity. Although compressive sensing algorithms based on angular sparsity can effectively reduce pilot overhead [128]–[130], the spherical wave characteristics of near-field propagation lead to significant energy dispersion in the angular domain, which can severely weaken its sparsity [20]. Therefore, compressive sensing algorithms relying on

angular sparsity developed for a far-field scenario may not be suitable for near-field channel estimation. In the following parts, we will first discuss channel estimation methods used in UE-BS near-field channel to address these challenges and provide effective solutions.

1) *For Single-User Single-Carrier Systems:* For the LoS channel in MISO systems, a promising strategy for the UE-BS channel estimation is to first recover the position of the UE, and subsequently incorporate these parameters into the parametric channel model to derive the channel estimate. This forms the basis of a parametric channel estimation approach. In this context, the authors of [22] effectively estimated the position of the UE in near-field THz channels by employing a 3-D multiple signal classification (MUSIC) algorithm. To further reduce the computational burden, a two-stage MUSIC algorithm was developed in [111]–[113]. In this approach, the DoA of the UE is first estimated, followed by the derivation of the distance between the UE and the BS using the acquired angular information. Additionally, the authors of [114] proposed a sequential angle-distance channel estimation (SADCE) method, which achieves position estimation accuracy comparable to that of the 3-D MUSIC algorithm, while substantially lowering computational complexity. Building upon these estimated position parameters, both [22] and [112] incorporated them into a near-field channel model to ultimately derive accurate channel estimates. Since parametric methods operate directly in the continuous parameter space, they typically offer high estimation accuracy; however, this often comes at the cost of increased computational complexity.

Furthermore, given the inherent sparsity of near-field channels in the polar domain, compressive sensing algorithms tailored to this domain have emerged as effective tools for estimating near-field multipath channels in MISO systems. These algorithms reconstruct the channel using a polar-domain codebook and sparse recovery techniques; therefore, the codebook design is critical for achieving accurate and efficient estimation. In [115], the subarray-wise and the scattering-wise channel estimation methods were proposed. The core idea is to partition the large-aperture array into multiple subarrays, each of which is processed independently using a refined OMP algorithm for accurate scatterer localization. Compared to conventional LS and standard OMP algorithms, this approach results in a significant improvement of the estimation accuracy. [83] introduced a triple parametric decomposition (TPD) framework, which constructs separate covariance matrices for azimuth-elevation angles and propagation distances, so as to achieve an independent parameter decomposition. By employing both on-grid and off-grid techniques, this method facilitates sparse recovery of angle and distance information without the energy leakage effect, while also reducing the complexity associated to the gridding operation. Apart from compressive sensing-based algorithms, works [116] and [117] proposed a variational Newtonized near-field channel estimation (VNNCE) algorithm for the multipath channel, achieving an estimation accuracy that approaches the relevant Cramér-Rao lower bound (CRLB). Moreover, for spatially correlated Rayleigh channels, [28] validated the effectiveness of the reduced subspace least squares (RS-LS) estimator under near-

TABLE IV: Estimation methods for BS-UE near-field channels in single-user systems.

System Type	Channel Type	Algorithm		Features	Reference	
Single-carrier	MISO	LoS	Parametric estimation method	3-D MUSIC algorithm	High accuracy and high complexity	[22]
				Two-stage MUSIC algorithm	High accuracy and low complexity	[111]–[113]
				SADCE method		[114]
		Multipath	Sparsity-aware method	Subarray-wise and the scattering-wise estimation methods based on the refined OMP	Enhanced estimation accuracy	[115]
				TPD framework	Leakage-free parameter estimation and low complexity	[83]
				VNNCE method		Estimation accuracy approaching the CRLB
	Rayleigh	RS-LS estimator		Validation of conventional estimators in the near-field case	[28]	
	MIMO	Multipath	Sparsity-aware method	Eigen-dictionary based on DPSS	Substantial reductions in baseband sampling and dictionary size	[118]
				OMP-based two-stage channel estimation	Performance approaching the CRLB	[27]
		Rician		3S-MMV framework based on unified OMP	Low complexity	[119]
Multi-carrier	MISO	LoS	Broadband beam training		Reduced pilot overhead	[76]
		Multipath	Sparsity-aware method	Adaptive JSBL-CE algorithm	Reduced codebook overhead	[120]
				AGSBL method	Enhanced estimation performance	[121]
			Deep learning method	CNN-based approach	Enhanced BER performance and reduced pilot overhead	[24]
				Mixed training strategy with DNN architecture	Low complexity and high robustness	[122]
				A-RCE network combined with TFIST	Enhanced estimation accuracy and reduced pilot overhead	[123]
		MIMO	LoS	Sparsity-aware method	D-STiCE method	Minimal pilot overhead
	Multipath		Parametric estimation method	Parametric SAGE algorithm	–	[125]

field conditions.

Extending to MIMO systems, [118] first applied a time reversal algorithm to localize UEs and scatterers in near-field multipath channels, and then designed an eigen-dictionary based on the discrete prolate spheroidal sequences (DPSS) via eigenvalue decomposition (EVD) of the channel matrix. This sparsity-aware design reduces baseband sampling by 51% and dictionary size by 66% compared to conventional DFT and spherical dictionaries. For Rician channels, [27] proposed a two-stage channel estimation algorithm, where the LoS component is estimated via coarse grid search followed by iterative refinement, while the NLoS components are recovered using OMP by exploiting the sparsity in the polar domain. The CRLB was also derived to assess the algorithm’s estimation performance. In [119], a low-overhead unified OMP (UOMP) estimation method was presented and further extended with a three-stage multiple-measurement-vector (3S-MMV) framework to reduce computational complexity. In summary, compared to parametric estimation methods, compressive sensing approaches typically offer lower computational complexity, although their estimation accuracy is limited by the resolution of the codebook.

2) *For Single-User Multi-Carrier Systems:* For orthogonal frequency division multiplexing (OFDM)-based MISO systems, [76] first demonstrated that near-field beams at different frequencies can be flexibly manipulated to cover distinct spatial regions. Leveraging this “near-field rainbow” effect, the authors proposed a fast broadband beam training method specifically designed for LoS channels, which achieves substantial reductions in training overhead while ensuring robust estimation of angles and distances.

Moreover, compressive sensing based on spatial sparsity also provide an effective approach for estimating near-field multipath channels in MISO-OFDM systems. The authors of [120] proposed an adaptive joint sparse Bayesian learning channel estimation (JSBL-CE) algorithm, which enables precise channel parameter estimation with reduced codebook overhead. In addition, [121] introduced an adaptive group

sparse Bayesian learning (AGSBL) method that incorporates a hierarchical prior model governed by tunable hyperparameters and employs a variational Bayesian algorithm. This method adaptively groups channels with similar sparsity patterns and exploits the partial joint sparsity within each group to achieve accurate channel estimation.

In addition to sparse Bayesian algorithms, deep learning methods also represent a promising approach for estimating near-field multipath channels. Compared to parametric estimation or compressive sensing methods, these approaches offer advantages in terms of computational complexity. In [24], a convolutional neural network (CNN)-based approach was proposed to estimate THz multiple channel parameters, including angles, distances, time delay and complex gains. This method outperforms conventional compressed sensing-based channel estimation algorithms in terms of bit error rate (BER) and pilot overhead. Furthermore, [122] proposed a deep unfolding-based algorithm specifically designed for channel estimation in THz multipath scenarios. This method mitigates the near-field beam split effect by employing frequency-dependent near-field dictionaries. A deep neural network (DNN) is also incorporated to learn optimal parameter updates in each iteration. Moreover, a mixed training strategy, combining the DNN architecture and loss function, is developed to enable low-complexity and highly robust estimation under various scenarios. To further leverage the complementary strengths of deep learning and sparsity-aware approaches, [123] proposed a deep learning-based joint channel estimation and sparse reconstruction scheme. An attention mechanism-based residual channel estimation (A-RCE) network is designed to enhance estimation accuracy by leveraging the inherent spatial correlations of the channel matrix across subcarriers and antennas. In parallel, a trainable fast iterative shrinkage-thresholding (TFIST) network is introduced to exploit the polar-domain sparsity of near-field channels, enabling a low-dimensional sparse representation and thereby reducing the overhead associated with CSI feedback.

Extending to the MIMO-OFDM scenario, [124] proposed

TABLE V: Estimation methods for BS-UE near-field channels in multi-user systems.

System Type	Channel Type			Algorithm	Features	Reference
Single-carrier	MISO	Multipath	Sparsity-aware method	Belief-based OMP method	Superior accuracy at low SNR	[131]
				cS-VBL and dS-VBL approaches	Higher accuracy and lower complexity than [121]	[132]
				Turbo-CoSaMP algorithm	High estimation accuracy	[133]
				Two-stage channel estimation based on SOMP and 2D-OMP	32% improvement in estimation accuracy over [133]	[134]
		MIMO			Grid-based polar-domain channel estimation	–
Multi-carrier	MISO	LoS	Sparsity-aware method	Two-level P-OMP algorithm	Superior performance over [136]	[137]
		Multipath	Sparsity-aware method	P-SOMP and P-SIGW hybrid estimation framework	Superior performance in terms of NMSE	[20]
				Inclusive P-SOMP method	Enhanced distance accuracy over [20]	[138]
				DL-OMP algorithm	Superior accuracy over P-OMP	[139]
				Beam-focused SOMP algorithm	–	[140]
				GP-SOMP and GP-SIGW algorithms	–	[136]
				CCSAMP-PR algorithm based on refined polar-domain dictionary	Mitigate the near-field beam-splitting effect in wideband systems	[141]
				NBA-OMP algorithm		[142]
				BPD-based method		[143]
			Segmented off-grid P-SIGW algorithm	[144]		
			Deep learning method	Neural network-based LIGW algorithm	Enhanced distance and channel recovery accuracy over [20]	[145]
				Dictionary learning-based bilevel optimization algorithm	Superior accuracy to P-SOMP [20] and lower complexity than BPD [143]	[146]
				FL-based framework	12× lower pilot overhead compared to [142]	[147]
				Two-stage channel estimation combining SOMP and GDM	Improved NMSE over LS and OMP	[148]
			Rician	Sparsity-aware method	Angular clustering-based estimation method	Outperforms P-SOMP in [20] while reducing complexity
		MIMO			–	

a deep sparse time-varying channel estimation (D-STiCe) method for the THz LoS channel. By leveraging long short-term memory (LSTM), this approach effectively captures the temporally correlated features of sparse channel parameters, enabling accurate estimation with minimal pilot overhead. For spatially non-stationary multipath channels, the authors of [125] proposed a parametric space-alternating generalized expectation-maximization (SAGE) algorithm for effective estimation of multi-bounce angular and distance parameters.

3) *For Multi-User Single-Carrier Systems:* Similarly, compressed sensing offers considerable potential for multipath channel estimation in multi-user MISO scenarios. [131] proposed a two-stage joint visibility region (VR) detection and channel estimation method. In the first stage, the VR detection-oriented message passing (VRDO-MP) approach is employed to estimate antenna visibility using spatial correlation. In the second stage, leveraging both VR information and wavenumber-domain sparsity, the belief-based OMP (BB-OMP) method is applied to estimate the multipath channel, achieving superior performance at low SNR. Furthermore, by leveraging the polar-domain sparsity, [132] proposed a decentralized channel estimation algorithm for multipath channels between the BS and multiple UEs. The algorithm first employs a centralized sub-array-based variational Bayesian learning (cS-VBL) approach and then extends it to a decentralized S-VBL (dS-VBL) implementation. Compared to the AGSBL algorithm in [121], the proposed approach achieves superior estimation accuracy with reduced computational complexity, thereby enhancing the overall SE. In [133], a polar-domain sparse channel sampling technique was integrated with the turbo-type compressive sampling matching pursuit (Turbo-CoSaMP) algorithm for channel estimation in massive un-sourced random access (URA) systems. By employing joint

angle-distance sampling, this method enhances channel sparsity. Besides, the Turbo-CoSaMP, which incorporates joint activity detection and channel estimation, iteratively identifies active codewords and estimates channel parameters. Furthermore, a Newton-based optimization procedure is incorporated into Turbo-CoSaMP to mitigate basis mismatch issues arising from discrete polar-domain sampling, thereby enabling more accurate multipath channel estimation. In [134], a two-stage channel estimation algorithm was developed. The first stage employs sparse OMP (SOMP) to estimate angle and distance parameters, while the second stage applies 2D-OMP for UE-path association. Compared to the Turbo-CoSaMP algorithm in [133], the proposed approach improves channel estimation accuracy by 32% without increasing computational complexity. [135] proposed a grid-based polar-domain channel estimation method, which is founded on the gradient descent approach and exploits the polar-domain sparsity of near-field channels. The performance of this method is further enhanced through the application of a deep unfolding technique.

4) *For Multi-User Multi-Carrier Systems:* For multi-user MISO-OFDM systems, sparsity-aware remains one of the effective approaches for near-field channel estimation. [150] proposed a dual-band near-field communication model to enhance the reconstructible sparsity of high-frequency near-field channels. By integrating structural characteristics derived from sparsity ambiguity with out-of-band spatial information from the low-frequency channel, this approach elevates the upper bound of sparsity reconstruction, thereby providing a foundation for the application of compressed sensing algorithms to channel estimation in multi-user and multi-carrier scenarios. Building on this, [20] introduced a hybrid estimation framework combining an on-grid polar-domain SOMP (P-SOMP) algorithm with an off-grid polar-domain

simultaneous iterative gridless weighted (P-SIGW) algorithm, achieving superior performance in terms of the normalized mean square error (NMSE). Extending the approach of [20], the authors of [138] proposed an inclusive P-SOMP method for jointly estimating angles, distances, and gains in near-field multipath channels, resulting in a significant enhancement in distance estimation accuracy compared to [20]. In parallel, [139] developed a distance-parameterized angular-domain sparse near-field channel model and proposed a dictionary learning orthogonal matching pursuit (DL-OMP) estimation method, applicable to both LoS and multipath scenarios. By employing joint dictionary learning and sparse recovery, the proposed approach achieves estimation accuracy superior to that of the conventional polar-domain OMP (P-OMP) method. In [140], a novel polar-domain codebook, independent of the user distance, was first designed to significantly reduce the codebook size. Using this optimized codebook, the authors proposed a beam-focused SOMP algorithm that effectively estimates near-field multipath channels. Furthermore, leveraging the fact that the multipath channels of different users share the same set of scatterers, the authors of [149] first estimated scatterer positions relative to a single reference user and then enabled other users to share these estimates, thereby reducing the overall computational complexity. To further enhance the accuracy of scatterer positioning, they also designed an angular clustering algorithm, which outperforms the P-SOMP method in [20]. In [136], a signal extraction method based on group time block coding (GTBC) was illustrated to capture spatial-domain non-stationarity in multipath channels. Building on the extracted signals, an on-grid GTBC-based polar-domain simultaneous OMP (GP-SOMP) algorithm and an off-grid GTBC-based polar-domain simultaneous iterative gridless weighted (GP-SIGW) algorithm were developed to achieve accurate estimation of multipath channels. On this basis, [137] introduced a two-level P-OMP algorithm and a list-based channel estimation method, demonstrating superior performance over [136].

Furthermore, to mitigate the near-field beam-splitting effect in wideband systems, the authors of [141] introduced a refined polar-domain dictionary for near-field multipath channels across different frequencies, enabling flexible adjustment of sampling angles and distances. They further proposed the correlation coefficient sparsity adaptive matching pursuit with parameter refinement (CCSAMP-PR) algorithm, which iteratively refines angle and distance estimates. This method achieves efficient near-field channel reconstruction with reduced complexity, even without exploiting any prior knowledge of channel sparsity. Similarly, in [142], a near-field beam-split aware OMP (NBA-OMP) algorithm was proposed for THz multipath channels. By constructing a dedicated NBA dictionary that accounts for angular and distance deviations, this approach effectively mitigates beam splitting over a 70 GHz bandwidth, achieving improved performance compared to [20]. Apart from these dictionary-based approaches, [143] presented a bilinear pattern detection (BPD)-based method to mitigate beam-splitting effects. This approach leverages linear frequency-dependent variations in the angular and distance domains to estimate the DoA and multipath distances across

frequencies. By incorporating compressed sensing, it enables the reconstruction of the entire wideband channel, delivering superior performance compared to existing methods reported in [20]. Following [143], [144] further developed a segmented off-grid P-SIGW algorithm, which further improves wideband channel estimation accuracy, achieving performance superior to that of the methods proposed in [20] and [143].

In addition to compressed sensing algorithms, deep learning techniques offer an effective solution for near-field channel estimation in multi-user and multi-carrier systems. The authors of [145] proposed a neural network-based localizer for initial near-field channel position estimation. The resulting channel estimate is further refined using a frequency-selectivity-based location-domain iterative gridless weighted (LIGW) method, which, compared to [20], demonstrates a remarkable improvement in both distance estimation and overall channel recovery accuracy. Besides, in [146], a dictionary learning-based bilevel optimization algorithm was introduced, in which an unsupervised deep neural network learns an optimal dictionary at the upper level, while the lower level identifies the best sparse representation of the near-field channel. Numerical results show that this approach not only outperforms the P-SOMP algorithm in [20] but also achieves lower computational complexity than the BPD method in [143]. Moreover, based on the model-based approach in [142], [147] developed a federated learning (FL)-based framework as a model-free alternative for multi-user channel estimation. By integrating labeled data from [142], this method reduces the training overhead by a factor of 12 compared to conventional techniques. Furthermore, by combining the complementary strengths of compressed sensing and deep learning techniques, [148] proposed a two-stage channel estimation method, where the SOMP is first used for coarse channel recovery. Then, treating the coarse estimate with errors as a noisy image, a generative deep model (GDM)-based approach is used to further refine the near-field channel estimate, achieving an improved NMSE over conventional LS and OMP methods.

In the preceding discussion, we have comprehensively reviewed the existing literature on the near-field BS-UE channel estimation across various scenarios. For ease of reference, the channel estimation methods for the *single-user* scenarios outlined in Sections IV-A(1) and IV-A(2) and the *multi-user* scenarios discussed in Sections IV-A(3) and IV-A(4) are summarized in Tables IV and V, respectively. From these tables, it can be observed that parametric channel estimation methods, compressed sensing algorithms, and deep learning techniques constitute the mainstream approaches for near-field channel estimation. The performance comparison of these three mainstream approaches is illustrated in Fig. 8. In general, parametric estimation methods offer high estimation accuracy and are particularly well-suited for channel models with deterministic structures, such as LoS and multipath scenarios. However, they typically involve searches over continuous parameter spaces, resulting in high computational complexity. Additionally, incorporating the estimated parameters into structured models makes them more sensitive to model mismatches. In contrast, compressive sensing techniques exploit the inherent sparsity of the channel and leverage structured

Criteria	Parametric Estimation	Sparsity-aware	Deep Learning
Applicable Channel	LoS/Multipath Channel	Sparse LoS/Multipath Channel	Multipath Channel in Multi-Carrier System
Estimation Accuracy	★★★★★	★★★★★	★★★★★
Computational Complexity	★★★★★	★★★★★	★★★★★
Robustness	★★★	★★★★★	★★★★★

Fig. 8: The performance comparison of mainstream estimation methods.

dictionary design to balance estimation accuracy and computational complexity effectively. These methods also exhibit moderate robustness, particularly in structured sparse channel environments. Deep learning-based methods, empowered by their strong representation and generalization capabilities, demonstrate enhanced robustness and improved computational efficiency, particularly in multi-carrier or complex propagation scenarios. In summary, these three approaches exhibit complementary trade-offs among estimation accuracy, computational complexity, and robustness, and should be selected based on the specific requirements and constraints of the deployment scenario. Although significant progress has been made in near-field BS-UE channel estimation across various system configurations, existing research has primarily focused on structurally deterministic channel models, such as LoS and multipath scenarios. In contrast, channel estimation techniques for statistically characterized models, such as the Rayleigh fading model, remain underexplored. Moreover, near-field channel estimation techniques tailored for multi-user MIMO scenarios are still limited and warrant further investigation and development.

B. XL-RIS-aided Near-Field Cascaded Channel Estimation

Building upon the research advances in direct channel estimation between the BS and UE, the subsequent sections systematically review near-field cascaded channel estimation methods in XL-RIS-aided wireless communications. The introduction of XL-RIS results in an exponential increase in the dimensionality of the cascaded channel. When combined with the nonlinear coupling of multi-dimensional parameters (e.g., distance, angle, and phase) induced by spherical wave propagation, this gives rise to a twofold computational challenge. On the one hand, due to the passive nature of the RIS, it cannot transmit or receive pilot signals directly. As a result, the cascaded channel must be estimated indirectly at the BS or the UE by appropriately adjusting the RIS reflection patterns. On the other hand, the strong coupling between parameters further complicates cascaded channel estimation, often requiring the solution of high-dimensional non-convex optimization problems. This typically involves large-scale matrix inversion and iterative optimization, significantly increasing computational

complexity. Consequently, the training overhead required for cascaded channel estimation grows exponentially with the number of RIS elements. In the following sections, we systematically summarize cascaded channel estimation methods applicable to various scenarios, with the aim of identifying effective solutions to the aforementioned challenges.

1) *For Single-User Single-Carrier Systems:* Similar to BS-UE channel estimation, sparsity-aware methods serve as effective tools for recovering multipath channels in RIS-aided MISO systems. The authors of [151] modeled the RIS-aided cascaded channel as a combination of a near-field multipath channel from the UE to the RIS and a far-field multipath channel from the RIS to the BS. Due to partial blockages, different visual regions (VRs) were assumed for each scatterer between the RIS and the UE. Based on this model, a two-stage strategy was proposed for joint channel and VR estimation leveraging a fast sparse Bayesian learning (FSBL) framework, which demonstrated superior performance compared to conventional OMP methods. Besides, in [152], a hybrid RIS is configured in which the elements located in the central subarray, as long as many specially selected discrete elements, are active, while all the others remain passive. For this architecture, a separate channel estimation scheme based on the decoupling operation (SCEDO) was proposed to estimate both the UE-RIS and RIS-BS multipath channels. In this process, a novel damped Newtonized orthogonal matching pursuit (DNOMP) algorithm with reduced computational complexity was developed. This algorithm combines planar and spherical wave models to estimate angle parameters using the central subarray, while recovering path gains and distances through the discrete elements. Similarly, a hybrid RIS structure combining both passive and active elements was discussed in [153], enabling the RIS to demodulate received pilot signals during training. Subsequently, by exploiting the block sparsity of the near-field channel, [153] proposed two low-complexity algorithms: the boundary estimation and sub-vector recovery (BESVR) algorithm and the linear total variation regularization (TVR) algorithm. Compared to the existing P-OMP method, both algorithms demonstrate significant advantages in terms of CPU time and NMSE. The work [103] further investigates the impact of various parameters, such as carrier frequency and RIS configuration, on the TVR algorithm proposed in [153], validating its applicability in the millimeter-wave band ($f_c = 28$ GHz). Extending to RIS-aided MIMO systems, in [155], a location estimation algorithm based on compressive sensing is designed to effectively retrieve the DoA and distance of the UE in the cascaded multipath channel. Through iterative design of the RIS phase-shifts, the positioning performance can be further improved.

In addition to sparsity-aware methods, low-rank algorithms offer a promising alternative for cascaded channel estimation in RIS-aided systems. These methods exploit the inherent redundancy of the channel matrix across spatial, temporal, or user domains. By modeling the channel as a low-rank or approximately low-rank structure, the high-dimensional estimation task can be decomposed into low-dimensional subspace learning and coefficient recovery. This reformulation significantly reduces computational complexity and training

TABLE VI: Estimation methods for RIS-aided near-field cascaded channels in single-user systems.

System Type	Channel Type	Algorithm		Features	Reference
Single-carrier	MISO	Sparsity-aware method	FSBL-based two-stage estimation strategy	Superior to OMP	[151]
			DNOMP-based separate channel estimation scheme	Reduced computational complexity	[152]
			BESVR and TVR algorithms	Lower CPU time and NMSE than P-OMP	[103], [153]
		Low-rank algorithm	PW-CLRA-based two-timescale estimation framework	Reduced pilot overhead and complexity	[154]
	MIMO	Sparsity-aware method	Compressive sensing-based localizer	–	[155]
Multi-carrier	MISO	Multipath	Sparsity-aware method	PF-RCE method	Superior estimation accuracy over OMP
				Polar bin design	1.2 dB NMSE gain over [25]
				3-D P-SOMP algorithm	96.9% pilot overhead reduction
	MIMO		2D-OLS-based MMPSR framework	Outperforms all existing 2-D reconstruction methods	[158]

overhead, while maintaining high estimation accuracy. In this context, the authors of [154] derived the time-scaling property of the cascaded channel in RIS-aided MISO systems, demonstrating that the channel can be represented as the product of large-timescale and small-timescale channels. Building on this foundation, they propose a two-timescale channel estimation (2TCE) framework: the large-timescale channel is estimated using the existing piece-wise collaborative low-rank approximation (PW-CLRA) algorithm [107], followed by the estimation of the small-timescale channel using observations from beam training together and the previously large-timescale estimation. This approach significantly reduces pilot overhead and computational complexity in RIS-aided cascaded channel estimation.

2) *For Single-User Multi-Carrier Systems:* Sparsity-aware methods also provide an effective solution for cascaded channel estimation in wideband systems. Leveraging the polar-domain sparsity of near-field multipath channels and the common sparsity support property of THz wideband channels, the authors of [25] proposed a novel polar-domain frequency-dependent RIS-aided channel estimation (PF-RCE) method for the THz MISO-OFDM system. Compared to existing OMP algorithms, PF-RCE demonstrates significantly improved estimation accuracy in wideband scenarios. Building upon this, the authors in [156] introduced a novel polar bin design to further enhance the sparse recovery performance of the PF-RCE, resulting in an additional 1.2 dB gain in terms of NMSE.

Extended to RIS-aided MIMO-OFDM systems, the authors of [157] proposed a 3-D P-SOMP algorithm for the cascaded multipath channel, which ensures accurate channel estimation while reducing the system pilot overhead by 96.9%. Moreover, the authors of [158] characterized the beam squint effect of wideband cascaded multipath channels in both the angular and distance domains and, based on this characterization, constructed a wideband spherical wave dictionary. Subsequently, a multi-frequency parallel subspace recovery (MMPSR) framework was developed, which transforms the 2-D compressed sensing problem into multiple sparse vector recovery problems and performs multi-frequency joint processing. Based on this framework, an atom matching method based on correlation coefficients was designed to replace the inner-product-based atom matching used in conventional OMP algorithms. In addition, the authors proposed a 2-D oracle least squares (2D-OLS) estimator, which ultimately achieved estimation accuracy surpassing all existing 2-D channel reconstruction methods.

3) *For Multi-User Single-Carrier Systems:* Similar to BS-UE channel estimation, the parametric estimation techniques provide an efficient approach for recovering cascaded channels in RIS-aided multi-user MISO systems. The authors of [159] proposed a low-overhead parametric channel reconstruction method for cascaded multipath channels. This approach introduces VR identification methods based on the accumulation function and sliding window by leveraging channel statistics, achieving centimeter-level joint localization for multiple users with a VR identification success rate exceeding 97%. The estimated user positions are subsequently incorporated into the cascaded channel model to accurately reconstruct the multipath channels of different users.

Moreover, sparsity-aware techniques also offer a promising solution for estimating cascaded channels in RIS-aided multi-user MISO systems. In [99], a polar domain dual-sparsity orthogonal matching pursuit (PDS-OMP) algorithm was combined with the LS estimator. This approach exploits the unique row-column sparsity of multi-user cascaded multipath channels in the polar domain, enabling accurate channel reconstruction with low pilot overhead. Besides, building on the row-column sparsity of multipath channels across users, [160] proposed a two-step joint multi-user channel estimation protocol. First, the received signal containing cascaded channel information from multiple users is projected onto a common column subspace by exploiting the shared column-block sparsity of the BS-RIS channel, reducing the channel matrix to one with only row-block sparsity. Then, an alternating optimization and iterative reweighted algorithm is applied to recover the joint sparse matrix, enabling more accurate estimation of the cascaded channels from different users.

Beyond sparsity-aware methods, deep learning has also emerged as a competitive approach for estimating cascaded channels across different users. The authors of [97] proposed a deep unfolding-based two-stage cascaded channel estimation strategy. In the first stage, a denoising convolutional neural network (DnCNN) is employed to estimate the angle and distance of the common path between the RIS and the BS. Subsequently, a network based on the iterative shrinkage-thresholding algorithm (ISTA) is designed to recover the angles, distances, and complex gains of the UE-RIS channels. Compared to existing OMP methods, the proposed approach demonstrates superior performance in terms of NMSE. In [161], a deep residual network-driven near-field cascaded channel estimation (DRN-NFCE) algorithm was developed. By leveraging the powerful feature-learning capability of deep learning techniques, the proposed DRN-NFCE network

TABLE VII: Estimation methods for RIS-aided near-field cascaded channels in multi-user systems.

System Type	Channel Type	Algorithm			Features	Reference
Single-carrier	MISO	Multipath	Parametric estimation method	VR identification based on accumulation function and sliding window	Centimeter-level UE localization and VR identification success rate > 97%	[159]
			Sparsity-aware method	PDS-OMP algorithm combined with LS	Low pilot overhead	[99]
		Deep learning method		Two-step estimation protocol	–	[160]
			Two-stage estimation strategy based on DnCNN and ISTA	Superior NMSE over OMP	[97]	
				DRN-NFCE algorithm	Higher accuracy and 80% pilot overhead reduction over LS and MMSE estimators	[161]
	Rayleigh	LMMSE-based three-stage estimation framework			Reduced pilot overhead	[162]
	MIMO	Multipath	Sparsity-aware method	Two-stage estimation protocol based on M-LAOMP and 3D-D-CS	Superior NMSE over OMP	[163]
			Low-rank algorithm	Two-step estimation framework based on CLRA-JO	80% training overhead reduction	[13]
Rician		Low-rank algorithm	Two-stage PW-CLRA algorithm	Higher accuracy and 70% training overhead reduction over [13]	[107]	
Multi-carrier	MISO	LoS	Parametric estimation method	Fresnel-based decoupled parametric estimation with a 2-D subspace method and a 1-D search	Reduced complexity	[164]
		Multipath	Sparsity-aware method	P-SOMP combined with P-SIGW	Improved accuracy over LS estimator	[165]
	MIMO	–				

achieves significantly higher estimation accuracy while reducing the pilot overhead by four-fifths compared to conventional LS and MMSE estimators.

In addition to the aforementioned methods, [162] proposed a three-stage cascaded channel estimation framework that exploits the fact that the cascaded channels of different users share a common RIS-BS channel. In the first two stages, a conventional LMMSE estimator is employed to estimate the UE-BS and UE-RIS-BS channels of a typical user, respectively. In the third stage, the UE-RIS-BS channels of the remaining users are recovered by leveraging the strong correlation between these channels and that of the typical user. This framework effectively reduces pilot overhead while maintaining high channel estimation accuracy.

Extended to MIMO systems, sparsity-aware approaches are also well-suited for acquiring CSI of RIS-aided multi-user cascaded channels. The authors of [163] proposed a two-stage channel estimation protocol based on compressed sensing. In the first stage, the 3-D and 2-D multiple measurement vector look-ahead orthogonal matching pursuit (M-LAOMP) algorithms sequentially estimate the common direction of departure (DoD) of the BS-RIS channel and the DoAs of different users. Based on these estimates, the 3-D distributed compressed sensing (3D-D-CS) framework is integrated with a compressed sensing approach based on the polar-domain dictionary in the second stage, to jointly recover the angle and distance information of the cascaded channels. Compared to conventional OMP algorithms, this approach significantly improves the NMSE performance.

Moreover, low-rank algorithms are also a potential approach for estimating the cascaded channels in RIS-aided multi-user MIMO systems. In [13], a two-step channel estimation framework based on the CLRA and joint optimization (CLRA-JO) was developed. The cascaded multipath channels between the UEs and the BS are first modeled as the product of a common column space matrix of the BS-RIS channel and user-specific coefficient matrices. Based on this model, the CLRA algorithm is employed to estimate the column space matrix, followed by the JO method to estimate the user-specific coefficient matrices. This approach ensures estimation accuracy while reducing the training overhead by approximately 80%. Moreover, the authors of [107] partitioned the

cascaded channels from different users into multiple piecewise channels that share low-rank subspaces and developed a two-stage PW-CLRA algorithm. In the first stage, training observations from different users are used to estimate the shared subspace, while in the second stage, the user-specific coefficient matrices are jointly optimized. Compared to the CLRA-JO method in [13], this approach improves estimation accuracy while reducing the training overhead by 70%.

4) *For Multi-User Multi-Carrier Systems:* Parametric channel estimation offers a competitive solution for recovering LoS channels in RIS-aided multi-user multi-carrier systems. In [164], a second-order Fresnel approximation was employed to decouple the angular and distance domains of the LoS channel, thereby reducing the complexity of cascaded channel estimation. Based on this decoupling, a 2-D subspace method and a 1-D search were applied to estimate the DoAs and distances of different UEs, respectively. Subsequently, a conventional LS method was used to recover the channel attenuation coefficients across the subcarriers, yielding a complete CSI. Moreover, similarly, sparsity-aware methods are also commonly employed for estimating cascaded multipath channels in this scenario. In [165], the P-SOMP algorithm is combined with the P-SIGW algorithm to perform joint channel estimation across multiple subcarriers, offering improved accuracy compared to the conventional LS estimator.

In this subsection, we provide a detailed discussion of existing cascaded channel estimation methods for RIS-aided near-field communications under various scenarios. For ease of reference, the cascaded channel estimation methods for *single-user* scenarios, as presented in Sections IV-B(1) and IV-B(2), and *multi-user* scenarios, as discussed in Sections IV-B(3) and IV-B(4), are summarized in Tables VI and VII, respectively. It is worth noting that parametric estimation, compressive sensing, and deep learning techniques, originally developed for BS-UE channel estimation, can be naturally extended to the RIS-aided cascaded channel estimation scenario. Beyond these mainstream approaches, the intrinsic redundancy of cascaded channels across the temporal or user domain makes low-rank algorithms a promising alternative. Compared with parametric estimation or sparsity-aware schemes, low-rank approaches offer comparable estimation accuracy, while substantially reducing pilot overhead and computational complexity

by exploiting low-dimensional subspace structures. Moreover, similar to BS-UE channel estimation, existing studies on RIS-aided cascaded channel estimation have primarily focused on scenarios with structurally deterministic channels, such as LoS or multipath models. In contrast, the investigation of cascaded channel estimation methods tailored for statistical channel models remains in its early stages and requires further exploration and refinement.

V. CONCLUSION AND FURTHER DISCUSSION

A. Conclusion

Under the evolution from massive MIMO to ELAAs, near-field transmission based on spherical wavefronts is expected to emerge as a fundamental paradigm in 6G wireless communications, where wireless channels must be jointly characterized by both angular and distance parameters. This joint dependency significantly increases the dimensionality of the near-field channel, posing new and unique challenges for accurate channel estimation. This survey has provided a comprehensive overview of near-field channel estimation solutions, encompassing a variety of system configurations and propagation scenarios. We first introduced the criteria for delineating far-field and near-field regions in antenna arrays, which serve as a foundation for near-field modeling. A detailed examination of existing modeling approaches was then presented, including near-field array response vectors, LoS and multipath channels, as well as spatial correlation-based models tailored to near-field characteristics. We further reviewed and analyzed various channel estimation techniques developed for both BS-to-UE direct channels and RIS-aided cascaded channels, covering a broad range of system configurations. It is hoped that this survey provides timely and valuable references to support and inspire future research and development in near-field channel estimation for 6G wireless communications.

B. Future Directions

As near-field channel estimation remains in its infancy, numerous critical challenges have yet to be addressed, warranting further in-depth investigation. Some potential directions for future research are outlined as follows:

- **Near-field channel estimation for statistically characterized models:** Existing near-field channel estimation techniques predominantly target deterministic channel models, such as LoS and sparse multipath scenarios, employing approaches like parametric estimation, compressed sensing, deep learning, and low-rank approximations. In contrast, estimation methods for statistically characterized channels, such as Rayleigh fading models, remain largely unexplored. Developing low-complexity, low-overhead algorithms tailored to such scenarios is an important and open research direction.
- **Dynamic near-field channel estimation:** Current near-field channel estimation techniques are mainly designed for quasi-static scenarios. However, in highly dynamic scenarios, such as those involving high-mobility users or interactive devices, the channel response exhibits rapid temporal variations and spatial non-stationarity. These

factors pose major challenges to conventional estimation methods in terms of both accuracy and computational complexity. Future research should focus on spatio-temporal joint modeling and predictive algorithms to better capture channel dynamics. Additionally, incorporating compressed pilot designs, mobility-aware strategies, and lightweight AI frameworks will be key to achieving efficient and robust estimation and tracking in dynamic near-field settings.

- **Near-field channel estimation for CAP arrays:** The advent of CAP arrays introduces strong mutual coupling effects due to their dense structural configuration, resulting in channel characteristics that deviate significantly from those of conventional SPD arrays. Consequently, existing channel estimation algorithms are not directly applicable to CAP-based systems. Despite this, near-field channel estimation for CAP arrays remains largely unexplored. Addressing this gap requires systematic advancements in channel modeling, estimation techniques, and hardware-aware algorithm design to support future near-field communication systems with high accuracy, low overhead, and strong robustness.

REFERENCES

- [1] S. Chen, C.-X. Wang, J. Li, C. Huang, H. Chang, Y. Huang, J. Huang, and Y. Chen, "Channel map-based angle domain multiple access for cell-free massive MIMO communications," *IEEE J. Sel. Top. Signal Process.*, vol. 19, no. 2, pp. 366–380, Mar. 2025.
- [2] Y. Liu, Z. Wang, J. Xu, C. Ouyang, X. Mu, and R. Schober, "Near-field communications: A tutorial review," *IEEE Open J. Commun. Soc.*, vol. 4, pp. 1999–2049, Aug. 2023.
- [3] H. Lu, Y. Zeng, C. You, Y. Han, J. Zhang, Z. Wang, Z. Dong, S. Jin, C.-X. Wang, T. Jiang *et al.*, "A tutorial on near-field XL-MIMO communications towards 6G," *IEEE Commun. Surveys Tuts.*, vol. 26, no. 4, p. 2213–2257, 4th Quart. 2024.
- [4] J. An, C. Yuen, L. Dai, M. Di Renzo, M. Debbah, and L. Hanzo, "Near-field communications: Research advances, potential, and challenges," *IEEE Wirel. Commun.*, vol. 31, no. 3, pp. 100–107, Jun. 2024.
- [5] ITU-R, "Framework and overall objectives of the future development of IMT for 2030 and beyond," Draft New Recommendation, Jun. 2023.
- [6] W.-X. Long, R. Chen, M. Moretti, W. Zhang, and J. Li, "A promising technology for 6G wireless networks: Intelligent reflecting surface," *J. Commun. Inf. Netw.*, vol. 6, no. 1, pp. 1–16, Mar. 2021.
- [7] C.-X. Wang, X. You, X. Gao, X. Zhu, Z. Li, C. Zhang, H. Wang, Y. Huang, Y. Chen, H. Haas, J. S. Thompson, E. G. Larsson, M. D. Renzo, W. Tong, P. Zhu, X. Shen, H. V. Poor, and L. Hanzo, "On the road to 6G: Visions, requirements, key technologies, and testbeds," *IEEE Commun. Surveys Tuts.*, vol. 25, no. 2, pp. 905–974, 2nd Quart. 2023.
- [8] E. Björnson, L. Sanguinetti, H. Wymeersch, J. Hoydis, and T. L. Marzetta, "Massive MIMO is a reality—What is next?: Five promising research directions for antenna arrays," *Digit. Signal Process.*, vol. 94, pp. 3–20, Nov. 2019.
- [9] S. Ye, M. Xiao, M.-W. Kwan, Z. Ma, Y. Huang, G. Karagiannidis, and P. Fan, "Extremely large aperture array (ELAA) communications: Foundations, research advances and challenges," *IEEE Open J. Commun. Soc.*, vol. 5, pp. 7075–7120, Oct. 2024.
- [10] W. Jiang, Q. Zhou, J. He, M. A. Habibi, S. Melnyk, M. El-Absi, B. Han, M. D. Renzo, H. D. Schotten, F.-L. Luo, T. S. El-Bawab, M. Juntti, M. Debbah, and V. C. M. Leung, "Terahertz communications and sensing for 6G and beyond: A comprehensive review," *IEEE Commun. Surv. Tutor.*, vol. 26, no. 4, pp. 2326–2381, Apr. 2024.
- [11] S. Thomas, J. Singh Viridi, A. Babakhani, and I. P. Roberts, "A survey on advancements in THz technology for 6G: Systems, circuits, antennas, and experiments," *IEEE Open J. Commun. Soc.*, vol. 6, pp. 1998–2016, Mar. 2025.
- [12] C.-X. Wang, J. Huang, H. Wang, X. Gao, X. You, and Y. Hao, "6G wireless channel measurements and models: Trends and challenges," *IEEE Veh. Technol. Mag.*, vol. 15, no. 4, pp. 22–32, Dec. 2020.

- [13] J. Lee, H. Chung, Y. Cho, S. Kim, and S. Hong, "Near-field channel estimation for XL-RIS assisted multi-user XL-MIMO systems: Hybrid beamforming architectures," *IEEE Trans. Wireless Commun.*, vol. 73, no. 3, pp. 1560–1574, Mar. 2025.
- [14] C. Han, Y. Wang, Y. Li, Y. Chen, N. A. Abbasi, T. Kürner, and A. F. Molisch, "Terahertz wireless channels: A holistic survey on measurement, modeling, and analysis," *IEEE Commun. Surv. Tutor.*, vol. 24, no. 3, pp. 1670–1707, Jun. 2022.
- [15] M. Cui, Z. Wu, Y. Lu, X. Wei, and L. Dai, "Near-field MIMO communications for 6g: Fundamentals, challenges, potentials, and future directions," *IEEE Commun. Mag.*, vol. 61, no. 1, pp. 40–46, Jan. 2023.
- [16] Y. Liu, C. Ouyang, Z. Wang, J. Xu, X. Mu, and A. L. Swindlehurst, "Near-field communications: A comprehensive survey," *IEEE Commun. Surv. Tutor.*, pp. 1–1, Oct. 2024.
- [17] Y. Liu, J. Xu, Z. Wang, X. Mu, and L. Hanzo, "Near-field communications: What will be different?" *IEEE Wirel. Commun.*, vol. 32, no. 2, pp. 262–270, Apr. 2025.
- [18] Y. Zheng, C.-X. Wang, J. Huang, R. Feng, and J. Thompson, "Measurements and characteristics analysis of 6G ultra-massive MIMO wireless channels with different antenna configurations and scenarios," *IEEE Trans. Veh. Technol.*, vol. 72, no. 8, pp. 9720–9732, Aug. 2023.
- [19] H. Zhang, N. Shlezinger, F. Guidi, D. Dardari, M. F. Imani, and Y. C. Eldar, "Beam focusing for near-field multiuser MIMO communications," *IEEE Trans. Wireless Commun.*, vol. 21, no. 9, pp. 7476–7490, Sep. 2022.
- [20] M. Cui and L. Dai, "Channel estimation for extremely large-scale MIMO: Far-field or near-field?" *IEEE Trans. Commun.*, vol. 70, no. 4, pp. 2663–2677, Apr. 2022.
- [21] Z. Dong and Y. Zeng, "Near-field spatial correlation for extremely large-scale array communications," *IEEE Commun. Lett.*, vol. 26, no. 7, pp. 1534–1538, Jul. 2022.
- [22] W.-X. Long, M. Moretti, M. Morelli, L. Sanguinetti, and R. Chen, "Parametric near-field MMSE channel estimation for sub-THz XL-MIMO systems," *arXiv preprint arXiv:2504.10064*, 2025.
- [23] H. Lei, J. Zhang, Z. Wang, B. Ai, and E. Björnson, "Near-field user localization and channel estimation for XL-MIMO systems: Fundamentals, recent advances, and outlooks," *IEEE Wirel. Commun.*, pp. 1–9, Jan. 2025.
- [24] A. Lee, H. Ju, S. Kim, and B. Shim, "Intelligent near-field channel estimation for terahertz ultra-massive MIMO systems," in *Proc. IEEE Global Commun. Conf. (GLOBECOM)*. IEEE, Dec. 2022, pp. 5390–5395.
- [25] J. Wu, S. Kim, and B. Shim, "Near-field channel estimation for RIS-assisted wideband terahertz systems," in *Proc. IEEE Global Commun. Conf. (GLOBECOM)*. IEEE, Dec. 2022, pp. 3893–3898.
- [26] M. Cui and L. Dai, "Near-field wideband beamforming for extremely large antenna arrays," *IEEE Trans. Wireless Commun.*, vol. 23, no. 10, pp. 13 110–13 124, Oct. 2024.
- [27] Y. Lu and L. Dai, "Near-field channel estimation in mixed LoS/NLoS environments for extremely large-scale MIMO systems," *IEEE Trans. Commun.*, vol. 71, no. 6, pp. 3694–3707, Jun. 2023.
- [28] Ö. T. Demir, A. Kosasih, and E. Björnson, "Spatial correlation modeling and rs-ls estimation of near-field channels with uniform planar arrays," in *2024 IEEE 25th International Workshop on Signal Processing Advances in Wireless Communications (SPAWC)*. IEEE, Sep. 2024, pp. 236–240.
- [29] S. Hu, H. Wang, and M. C. Ilter, "Design of near-field beamforming for large intelligent surfaces," *IEEE Trans. Wireless Commun.*, vol. 23, no. 1, pp. 762–774, Jan. 2023.
- [30] Y. Han, S. Jin, M. Matthaiou, T. Q. Quek, and C.-K. Wen, "Toward extra large-scale MIMO: New channel properties and low-cost designs," *IEEE Internet Things J.*, vol. 10, no. 16, pp. 14 569–14 594, Aug. 2023.
- [31] P. Lemaître-Auger, R. Siragusa, C. Caloz, and D. Kaddour, "Circular antenna arrays for near-field focused or multi-focused beams," in *Proc. 2013 URSI Int. Symp. Electromagnetic Theory*. IEEE, 2013, pp. 425–428.
- [32] Y. Xie, B. Ning, L. Li, and Z. Chen, "Near-field beam training in THz communications: The merits of uniform circular array," *IEEE Wireless Commun. Lett.*, vol. 12, no. 4, pp. 575–579, Apr. 2023.
- [33] A. Kay, "Near-field gain of aperture antennas," *IEEE Trans. Antennas Propag.*, vol. 8, no. 6, pp. 586–593, Nov. 1960.
- [34] Y. Wang, C. Han, S. Sun, and J. Zhang, "Cross far-and near-field channel measurement and modeling in extremely large-scale movable antenna array systems," *IEEE Trans. Antennas Propag.*, 2025.
- [35] K. T. Selvan and R. Janaswamy, "Fraunhofer and fresnel distances: Unified derivation for aperture antennas," *IEEE Antennas Propag. Mag.*, vol. 59, no. 4, pp. 12–15, Aug. 2017.
- [36] J. Li, Y. Wang, Z. Ren, X. Gu, M. Yin, and Z. Wu, "DOA and range estimation using a uniform linear antenna array without a priori knowledge of the source number," *IEEE Trans. Antenn. Propag.*, vol. 69, no. 5, pp. 2929–2939, May 2020.
- [37] C. Polk, "Optical fresnel-zone gain of a rectangular aperture," *IRE Trans. Antennas Propag.*, vol. 4, no. 1, pp. 65–69, Jan. 1956.
- [38] H. Lu and Y. Zeng, "Communicating with extremely large-scale array/surface: Unified modeling and performance analysis," *IEEE Trans. Wireless Commun.*, vol. 21, no. 6, pp. 4039–4053, Jun. 2021.
- [39] Z. Wang, J. Zhang, H. Du, D. Niyato, S. Cui, B. Ai, M. Debbah, K. B. Letaief, and H. V. Poor, "A tutorial on extremely large-scale MIMO for 6G: Fundamentals, signal processing, and applications," *IEEE Commun. Surv. Tuts.*, p. 1561, Jan. 2024.
- [40] I. Yoo, M. F. Imani, T. Slesman, H. D. Pfister, and D. R. Smith, "Enhancing capacity of spatial multiplexing systems using reconfigurable cavity-backed metasurface antennas in clustered MIMO channels," *IEEE Trans. Commun.*, vol. 67, no. 2, pp. 1070–1084, Feb. 2018.
- [41] H. Wang, N. Shlezinger, S. Jin, Y. C. Eldar, I. Yoo, M. F. Imani, and D. R. Smith, "Dynamic metasurface antennas based downlink massive MIMO systems," in *Proc. IEEE 20th Int. Workshop Signal Process. Adv. Wireless Commun. (SPAWC)*. IEEE, Aug. 2019, pp. 1–5.
- [42] N. Shlezinger, O. Dicker, Y. C. Eldar, I. Yoo, M. F. Imani, and D. R. Smith, "Dynamic metasurface antennas for uplink massive MIMO systems," *IEEE Trans. Commun.*, vol. 67, no. 10, pp. 6829–6843, Oct. 2019.
- [43] N. Shlezinger, G. C. Alexandropoulos, M. F. Imani, Y. C. Eldar, and D. R. Smith, "Dynamic metasurface antennas for 6G extreme massive MIMO communications," *IEEE Wireless Commun.*, vol. 28, no. 2, pp. 106–113, Apr. 2021.
- [44] C. Huang, A. Zappone, G. C. Alexandropoulos, M. Debbah, and C. Yuen, "Reconfigurable intelligent surfaces for energy efficiency in wireless communication," *IEEE Trans. Wireless Commun.*, vol. 18, no. 8, pp. 4157–4170, Aug. 2019.
- [45] L. Dai, B. Wang, M. Wang, X. Yang, J. Tan, S. Bi, S. Xu, F. Yang, Z. Chen, M. Di Renzo *et al.*, "Reconfigurable intelligent surface-based wireless communications: Antenna design, prototyping, and experimental results," *IEEE Access*, vol. 8, pp. 45 913–45 923, Mar. 2020.
- [46] S. Venkatesh, X. Lu, H. Saeidi, and K. Sengupta, "A high-speed programmable and scalable terahertz holographic metasurface based on tiled CMOS chips," *Nature Electron.*, vol. 3, no. 12, pp. 785–793, Dec. 2020.
- [47] A. Araghi, M. Khalily, M. Safaei, A. Bagheri, V. Singh, F. Wang, and R. Tafazolli, "Reconfigurable intelligent surface (RIS) in the sub-6 GHz band: Design, implementation, and real-world demonstration," *IEEE Access*, vol. 10, pp. 2646–2655, Jan. 2022.
- [48] M. E. Badawe, T. S. Almonief, and O. M. Ramahi, "A true metasurface antenna," *Sci. Rep.*, vol. 6, no. 1, p. 19268, Jan. 2016.
- [49] O. Yurduseven, D. L. Marks, J. N. Gollub, and D. R. Smith, "Design and analysis of a reconfigurable holographic metasurface aperture for dynamic focusing in the Fresnel zone," *IEEE Access*, vol. 5, pp. 15 055–15 065, Jun. 2017.
- [50] O. Yurduseven, D. L. Marks, T. Fromenteze, and D. R. Smith, "Dynamically reconfigurable holographic metasurface aperture for a Mills-Cross monochromatic microwave camera," *Opt. Express*, vol. 26, no. 5, pp. 5281–5291, 2018.
- [51] I. Yoo and D. R. Smith, "Holographic metasurface antennas for uplink massive MIMO systems," *arXiv preprint arXiv:2108.12513*, 2021.
- [52] S. Foo, "Liquid-crystal reconfigurable metasurface reflectors," in *Proc. IEEE Int. Symp. Antennas Propag., USNC/URSI Nat. Radio Sci. Meeting*. IEEE, Oct. 2017, pp. 2069–2070.
- [53] S. Hu and F. Rusek, "Spherical large intelligent surfaces," in *Proc. IEEE Int. Conf. Acoust., Speech Signal Process. (ICASSP)*. IEEE, Apr. 2020, pp. 8673–8677.
- [54] X. Li, J. Fang, F. Gao, and H. Li, "Joint active and passive beamforming for intelligent reflecting surface-assisted massive MIMO systems," *arXiv:1912.00728*. [Online]. Available: <http://arxiv.org/abs/1912.00728>, 2019.
- [55] Q. Wu and R. Zhang, "Intelligent reflecting surface enhanced wireless network via joint active and passive beamforming," *IEEE Trans. Wireless Commun.*, vol. 18, no. 11, pp. 5394–5409, Nov. 2019.
- [56] B. Di, H. Zhang, L. Song, Y. Li, Z. Han, and H. V. Poor, "Hybrid beamforming for reconfigurable intelligent surface based multi-user communications: Achievable rates with limited discrete phase shifts,"

- IEEE J. Sel. Areas Commun.*, vol. 38, no. 8, pp. 1809–1822, Aug. 2020.
- [57] J. Xu, L. You, G. C. Alexandropoulos, X. Yi, W. Wang, and X. Gao, “Near-field wideband extremely large-scale MIMO transmissions with holographic metasurface-based antenna arrays,” *IEEE Trans. Wireless Commun.*, vol. 23, no. 9, pp. 12 054 – 12 067, Sep. 2024.
 - [58] W. Yan, X. Yuan, and X. Kuai, “Passive beamforming and information transfer via large intelligent surface,” *IEEE Wireless Commun. Lett.*, vol. 9, no. 4, pp. 533–537, Apr. 2019.
 - [59] J. A. Zhang, X. Huang, V. Dyadyuk, and Y. J. Guo, “Massive hybrid antenna array for millimeter-wave cellular communications,” *IEEE Wireless Commun.*, vol. 22, no. 1, pp. 79–87, Feb. 2015.
 - [60] J. Zhang, X. Huang, V. Dyadyuk, and Y. J. Guo, “Hybrid antenna array for mmwave massive MIMO,” in *mmWave Massive MIMO: A Paradigm for 5G*. Elsevier, 2017, pp. 39–61.
 - [61] V. Arun and H. Balakrishnan, “{RFocus}: Beamforming using thousands of passive antennas,” in *Proc. 17th USENIX Symp. Networked Systems Design and Implementation*, 2020, pp. 1047–1061.
 - [62] Z. Wan, Z. Gao, F. Gao, M. Di Renzo, and M.-S. Alouini, “Terahertz massive MIMO with holographic reconfigurable intelligent surfaces,” *IEEE Trans. Commun.*, vol. 69, no. 7, pp. 4732–4750, Jul. 2021.
 - [63] H. Yang, X. Cao, F. Yang, J. Gao, S. Xu, M. Li, X. Chen, Y. Zhao, Y. Zheng, and S. Li, “A programmable metasurface with dynamic polarization, scattering and focusing control,” *Sci. Rep.*, vol. 6, no. 1, pp. 1–11, Oct. 2016.
 - [64] L. Zhang, X. Q. Chen, S. Liu, Q. Zhang, J. Zhao, J. Y. Dai, G. D. Bai, X. Wan, Q. Cheng, G. Castaldi *et al.*, “Space-time-coding digital metasurfaces,” *Nat. Commun.*, vol. 9, no. 1, p. 4334, Oct. 2018.
 - [65] X. G. Zhang, W. X. Jiang, H. L. Jiang, Q. Wang, H. W. Tian, L. Bai, Z. J. Luo, S. Sun, Y. Luo, C.-W. Qiu *et al.*, “An optically driven digital metasurface for programming electromagnetic functions,” *Nat. Electron.*, vol. 3, no. 3, pp. 165–171, Mar. 2020.
 - [66] J. R. Sánchez, F. Rusek, O. Edfors, and L. Liu, “Distributed and scalable uplink processing for LIS: Algorithm, architecture, and design trade-offs,” *IEEE Trans. Signal Process.*, vol. 70, pp. 2639–2653, 2022.
 - [67] I. Ahmed, H. Khammari, A. Shahid, A. Musa, K. S. Kim, E. De Poorter, and I. Moerman, “A survey on hybrid beamforming techniques in 5G: Architecture and system model perspectives,” *IEEE Commun. Surveys Tuts.*, vol. 20, no. 4, pp. 3060–3097, 4th Quart. 2018.
 - [68] G. C. Nwaloze, D. Rakhimov, and M. Haardt, “Near-field beamforming for MU-MIMO millimeter wave communication system,” in *2023 31st European Signal Processing Conference (EUSIPCO)*. IEEE, Sep. 2023, pp. 1683–1687.
 - [69] O. El Ayach, S. Rajagopal, S. Abu-Surra, Z. Pi, and R. W. Heath, “Spatially sparse precoding in millimeter wave MIMO systems,” *IEEE Trans. Wireless Commun.*, vol. 13, no. 3, pp. 1499–1513, Mar. 2014.
 - [70] X. Yu, J. C. Shen, J. Zhang, and K. B. Letaief, “Hybrid precoding design in millimeter wave MIMO systems: An alternating minimization approach,” in *Proc. IEEE Glob. Commun. Conf.* IEEE, Apr. 2015, pp. 1–6.
 - [71] X. Yu, J.-C. Shen, J. Zhang, and K. B. Letaief, “Alternating minimization algorithms for hybrid precoding in millimeter wave MIMO systems,” *IEEE J. Sel. Topics Signal Process.*, vol. 10, no. 3, pp. 485–500, Apr. 2016.
 - [72] F. Sohrabi and W. Yu, “Hybrid digital and analog beamforming design for large-scale MIMO systems,” in *Proc. IEEE Int. Conf. Acoust. Speech Signal Process.* IEEE, 2015, pp. 2929–2933.
 - [73] Z. Zhang, Y. Liu, Z. Wang, J. Chen, and T. Q. Quek, “Dynamic MIMO architecture design for near-field communications,” *IEEE Trans. Wireless Commun.*, vol. 23, no. 10, pp. 14 669–14 684, Oct. 2024.
 - [74] J. Wang, J. Xiao, Y. Zou, W. Xie, and Y. Liu, “Wideband beamforming for RIS assisted near-field communications,” *IEEE Trans. Wireless Commun.*, 2024.
 - [75] J. Sherman, “Properties of focused apertures in the fresnel region,” *IRE Trans. on Antennas and Propag.*, vol. 10, no. 4, pp. 399–408, Jul. 1962.
 - [76] M. Cui, L. Dai, Z. Wang, S. Zhou, and N. Ge, “Near-field rainbow: Wideband beam training for XL-MIMO,” *IEEE Trans. Wireless Commun.*, vol. 22, no. 6, pp. 3899–3912, Jun. 2022.
 - [77] A. Kosasih, Ö. T. Demir, N. Kolomvakis, and E. Björnson, “The roles of spatial frequencies and degrees-of-freedom in near-field communications,” *arXiv preprint arXiv:2407.07448*, Jul. 2024.
 - [78] Z. Dong, X. Li, Y. Zeng, S. Jin, and T. Jiang, “Near-field spatial correlation for multi-path XL-array communications with partial visibility,” in *Proc. IEEE Global Commun. Conf. (GLOBECOM)*. IEEE, Dec. 2023, pp. 1525–1530.
 - [79] J. Liu, Y. Ma, J. Wang, N. Yi, R. Tafazolli, S. Xue, and F. Wang, “A non-stationary channel model with correlated NLoS/LoS states for ELAA-mMIMO,” in *Proc. IEEE Global Commun. Conf. (GLOBECOM)*. IEEE, Dec. 2021, pp. 1–6.
 - [80] J. Liu, Y. Ma, and R. Tafazolli, “A spatially non-stationary fading channel model for simulation and (semi-) analytical study of ELAA-MIMO,” *IEEE Trans. Wireless Commun.*, vol. 23, no. 5, pp. 5203 – 5218, May 2023.
 - [81] B. Zhao, C. Ouyang, X. Zhang, and Y. Liu, “Performance analysis of near-field ISAC based on an accurate channel model,” in *Proc. IEEE Int. Commun. Conf. (ICC)*. IEEE, Oct. 2024, pp. 4918–4923.
 - [82] Z. Lu, Y. Han, S. Jin, and M. Matthaiou, “Near-field localization and channel reconstruction for ELAA systems,” *IEEE Trans. Wireless Commun.*, vol. 23, no. 7, pp. 6938 – 6953, Jul. 2023.
 - [83] X. Guo, Y. Chen, and Y. Wang, “Compressed channel estimation for near-field XL-MIMO using triple parametric decomposition,” *IEEE Trans. Veh. Technol.*, vol. 72, no. 11, pp. 15 040–15 045, Nov. 2023.
 - [84] W. Wang, Z. Lian, Y. Wang, and Y. Su, “Geometry-based channel model for extra-large scale array communication systems,” *IEEE Wireless Commun. Lett.*, vol. 13, no. 4, pp. 1014–1018, Apr. 2024.
 - [85] Y. Ji, W. Fan, and G. F. Pedersen, “Near-field signal model for large-scale uniform circular array and its experimental validation,” *IEEE Antennas Wireless Propag. Lett.*, vol. 16, pp. 1237–1240, 2016.
 - [86] B. Qin, F. Zhou, W. Zhang, C. You, and B. Zheng, “Fast distance sampling for uniform circular array in near-field 3D beam-focusing,” *IEEE Signal Process. Lett.*, vol. 31, pp. 2210 – 2214, 2024.
 - [87] Z. Wu, M. Cui, and L. Dai, “Enabling more users to benefit from near-field communications: From linear to circular array,” *IEEE Trans. Wireless Commun.*, vol. 23, no. 4, pp. 3735 – 3748, Apr. 2023.
 - [88] Y. Chen and L. Dai, “Near-field wideband beam training for ELAA with uniform circular array,” *Sci. China Inf. Sci.*, vol. 67, no. 6, pp. 1–14, 2024.
 - [89] J. Peng and Y. Wang, “Near-field channel estimation for extremely large antenna arrays with uniform circular arrays,” *IEEE Access*, pp. 1–1, 2024.
 - [90] Y. He, C.-X. Wang, H. Chang, R. Feng, J. Sun, W. Zhang, Y. Hao, and E.-H. M. Aggoune, “A novel 3-D beam domain channel model for maritime massive MIMO communication systems using uniform circular arrays,” *IEEE Trans. Commun.*, vol. 71, no. 4, pp. 2487–2502, Apr. 2023.
 - [91] J. Tian, Y. Han, S. Jin, J. Zhang, and J. Wang, “Analytical channel modeling: From MIMO to extra large-scale MIMO,” *Chin. J. Electron.*, vol. 34, no. 1, pp. 1–15, May 2025.
 - [92] H. Jiang, W. Shi, X. Chen, Q. Zhu, and Z. Chen, “High-efficient near-field channel characteristics analysis for large-scale MIMO communication systems,” *IEEE Internet Things J.*, early access, 2024.
 - [93] C.-X. Wang, Z. Lv, Y. Chen, and H. Haas, “A complete study of space-time-frequency statistical properties of the 6G pervasive channel model,” *IEEE Trans. Commun.*, vol. 71, no. 12, pp. 7273–7287, Dec. 2023.
 - [94] Y. Zheng, C.-X. Wang, R. Yang, L. Yu, F. Lai, J. Huang, R. Feng, C. Wang, C. Li, and Z. Zhong, “Ultra-massive MIMO channel measurements at 5.3 GHz and a general 6G channel model,” *IEEE Trans. Veh. Technol.*, vol. 72, no. 1, pp. 20–34, Jan. 2023.
 - [95] C.-X. Wang, Z. Lv, C. Huang, Y. Huang, J. Wang, J. Huang, and X. You, “An enhanced 6G pervasive channel model towards standardization,” *Sci. China Inf. Sci.*, vol. 68, no. 6, pp. 162 301:1–162 301:22, Jun. 2025.
 - [96] K. Dovelos, S. D. Assimonis, H. Q. Ngo, B. Bellalta, and M. Matthaiou, “Intelligent reflecting surfaces at terahertz bands: Channel modeling and analysis,” in *Proc. IEEE Int. Conf. Commun. Workshops (ICC Workshops)*. IEEE, Jun. 2021, pp. 1–6.
 - [97] Z. Tang, Y. Chen, Y. Wang, T. Mao, Q. Wu, M. Di Renzo, and L. Hanzo, “Near-field sparse channel estimation for extremely large-scale RIS-aided wireless communications,” in *Proceedings of IEEE Globecom Workshops*. IEEE, 2023, pp. 1373–1379.
 - [98] W. Liu, C. Pan, H. Ren, F. Shu, S. Jin, and J. Wang, “Low-overhead beam training scheme for extremely large-scale RIS in near field,” *IEEE Trans. Commun.*, vol. 71, no. 8, pp. 4924–4940, Aug. 2023.
 - [99] Y. Jin and H. Qi, “Near-field channel estimation for RIS assisted 6G wireless communication,” in *Proc. IEEE Int. Conf. Signal Process. Commun. Comput. (ICSPCC)*. IEEE, Apr. 2023, pp. 1–6.
 - [100] Y. Chen, M. Jian, and L. Dai, “Channel estimation for RIS assisted wireless communications: Stationary or non-stationary?” *IEEE Trans. Signal Process.*, vol. 72, pp. 3776 – 3791, 2024.

- [101] M. Rahal, B. Denis, M. F. Keskin, B. Uguen, and H. Wymeersch, "RIS-enabled NLoS near-field joint position and velocity estimation under user mobility," *IEEE J. Sel. Topics Signal Process.*, 2024.
- [102] Y. Yuan, Y. Chen, X. Guo, and Y. Wang, "Near-field tracking with extremely large-scale RIS: A sparse learning approach," in *2024 IEEE Wireless Communications and Networking Conference (WCNC)*. IEEE, 2024, pp. 1–6.
- [103] R. Schroeder, J. He, and M. Juntti, "Near-field channel estimation for extremely-large single-RF-chain RIS systems," in *2024 IEEE 25th International Workshop on Signal Processing Advances in Wireless Communications (SPAWC)*. IEEE, 2024, pp. 266–270.
- [104] J. Tian, Y. Han, S. Jin, X. Li, J. Zhang, and M. Matthaiou, "Near-field channel reconstruction in sensing RIS-assisted wireless communication systems," *IEEE Trans. Wireless Commun.*, vol. 23, no. 9, p. 12223–12238, Sept. 2024.
- [105] G. Bartoli, A. Abrardo, N. Decarli, D. Dardari, and M. Di Renzo, "Spatial multiplexing in near field MIMO channels with reconfigurable intelligent surfaces," *IET Signal Process.*, vol. 17, no. 3, p. e12195, Mar. 2023.
- [106] X. Zhang, H. Shao, W. Zhang, Z. Xie, X. Yang, and W. Jing, "RIS-aided XL-MIMO channel estimation based on expectation-maximization," *IEEE Commun. Lett.*, 2024.
- [107] J. Lee and S. Hong, "Near-field LoS/NLoS channel estimation for RIS-aided MU-MIMO systems: Piece-wise low-rank approximation approach," *IEEE Trans. Commun.*, 2025.
- [108] S. Lv, Y. Liu, X. Xu, A. Nallanathan, and A. L. Swindlehurst, "RIS-aided near-field MIMO communications: Codebook and beam training design," *IEEE Trans. Wireless Commun.*, vol. 23, no. 9, pp. 12 531 – 12 546, Sept. 2024.
- [109] T. Gong, L. Wei, C. Huang, G. C. Alexandropoulos, M. Debbah, and C. Yuen, "Near-field channel modeling for holographic MIMO communications," *IEEE Wirel. Commun.*, vol. 31, no. 3, pp. 108–116, Jun. 2024.
- [110] S. Wu, C.-X. Wang, e.-H. M. Aggoune, M. M. Alwakeel, and Y. He, "A non-stationary 3-D wideband twin-cluster model for 5G massive MIMO channels," *IEEE J. Sel. Areas Commun.*, vol. 32, no. 6, pp. 1207–1218, Jun. 2014.
- [111] J. He, M. N. S. Swamy, and M. O. Ahmad, "Efficient application of MUSIC algorithm under the coexistence of far-field and near-field sources," *IEEE Trans. Signal Process.*, vol. 60, no. 4, pp. 2066–2070, Apr. 2012.
- [112] A. Kosasih, Ö. T. Demir, and E. Björnson, "Parametric near-field channel estimation for extremely large aperture arrays," in *2023 57th Asilomar Conference on Signals, Systems, and Computers*. IEEE, Oct. 2023, pp. 162–166.
- [113] K. Qu, S. Guo, J. Ye, and H. Zhao, "Two-stage beamspace MUSIC-based near-field channel estimation for hybrid XL-MIMO," *IEEE Commun. Lett.*, vol. 28, no. 8, pp. 1949–1953, Aug. 2024.
- [114] C. Huang, J. Xu, W. Xu, X. You, C. Yuen, and Y. Chen, "Low-complexity channel estimation for extremely large-scale MIMO in near field," *IEEE Wirel. Commun. Lett.*, vol. 13, no. 3, pp. 671 – 675, Mar. 2023.
- [115] Y. Han, S. Jin, C.-K. Wen, and X. Ma, "Channel estimation for extremely large-scale massive MIMO systems," *IEEE Wirel. Commun. Lett.*, vol. 9, no. 5, pp. 633–637, May 2020.
- [116] R. Cao, H. He, X. Yu, S. Song, K. Huang, J. Zhang, Y. Gong, and K. B. Letaief, "Joint channel estimation and cooperative localization for near-field ultra-massive MIMO," *arXiv preprint arXiv:2312.13683*, 2023.
- [117] R. Cao, W. Yu, H. He, X. Yu, S. Song, J. Zhang, Y. Gong, and K. B. Letaief, "Newtonized near-field channel estimation for ultra-massive MIMO systems," in *2024 IEEE Wireless Communications and Networking Conference (WCNC)*. IEEE, 2024, pp. 1–6.
- [118] S. Liu, X. Yu, Z. Gao, J. Xu, D. W. K. Ng, and S. Cui, "Sensing-enhanced channel estimation for near-field XL-MIMO systems," *IEEE J. Sel. Areas Commun.*, vol. 43, no. 3, pp. 628 – 643, Mar. 2025.
- [119] X. Shi, J. Wang, X. Wang, C. You, and J. Song, "Double-sided near-field XL-MIMO: Beamfocusing codeword selection and channel estimation," *IEEE Trans. Commun.*, early access, 2024.
- [120] Z. Zhu, R. Yang, J. Zhang, S. Xu, C. Li, Y. Huang, and L. Yang, "Sparse bayesian learning-based adaptive codebook for near-field channel estimation," in *ICC 2024-IEEE International Conference on Communications*. IEEE, 2024, pp. 2366–2371.
- [121] X. Cheng, K. Xu, J. Sun, and S. Li, "Adaptive grouping sparse bayesian learning for channel estimation in non-stationary uplink massive MIMO systems," *IEEE Trans. Wireless Commun.*, vol. 18, no. 8, pp. 4184–4198, Aug. 2019.
- [122] J. Gao, X. Chen, and G. Y. Li, "Deep unfolding based channel estimation for wideband terahertz near-field massive MIMO systems," *Frontiers of Information Technology & Electronic Engineering(FITEE)*, vol. 25, no. 8, pp. 1162–1172, 2024.
- [123] Z. Wang, G. Zhang, J. Wang, and H. Xu, "Near-field channel estimation and sparse reconstruction for FDD XL-MIMO systems," *IEEE Commun. Lett.*, pp. 1–1, Feb. 2025.
- [124] J. Kim, Y. Ahn, S. Kim, and B. Shim, "Deep learning-aided parametric sparse channel estimation for terahertz massive MIMO systems," *IEEE Trans. Cogn. Commun. Netw.*, vol. 10, no. 6, pp. 2136 – 2148, Dec. 2024.
- [125] Y. Liu, L. Wu, X. Cai, and M. B. Shankar, "Graph-based multi-bounce modeling and channel parameter estimation for indoor sensing," *IEEE Transactions on Wireless Communications, Early Access*, pp. 1–1, 2025.
- [126] W.-X. Long, M. Moretti, L. Sanguinetti, and R. Chen, "Channel estimation in RIS-aided communications with interference," *IEEE Wirel. Commun. Lett.*, vol. 12, no. 10, pp. 1751–1755, Oct. 2023.
- [127] W.-X. Long, M. Moretti, A. Abrardo, L. Sanguinetti, and R. Chen, "Mmse design of RIS-aided communications with spatially-correlated channels and electromagnetic interference," *IEEE Trans. Wireless Commun.*, vol. 23, no. 11, pp. 16 992–17 006, Nov. 2024.
- [128] J. Tao, C. Qi, and Y. Huang, "Regularized multipath matching pursuit for sparse channel estimation in millimeter wave massive MIMO system," *IEEE Wirel. Commun. Lett.*, vol. 8, no. 1, pp. 169–172, Feb. 2018.
- [129] X. Wei, C. Hu, and L. Dai, "Deep learning for beamspace channel estimation in millimeter-wave massive MIMO systems," *IEEE Trans. Wireless Commun.*, vol. 69, no. 1, pp. 182–193, Jan. 2020.
- [130] H. Lei, J. Zhang, Z. Wang, B. Ai, and E. Björnson, "Near-field user localization and channel estimation for XL-MIMO systems: Fundamentals, recent advances, and outlooks," *IEEE Wirel. Commun., early access*, pp. 1–9, 2025.
- [131] A. Tang, J.-B. Wang, Y. Pan, W. Zhang, X. Zhang, Y. Chen, H. Yu, and R. C. De Lamare, "Joint visibility region and channel estimation for extremely large-scale MIMO systems," *IEEE Trans. Commun.*, vol. 72, no. 10, pp. 6087 – 6101, Oct. 2024.
- [132] J. N. Pisharody, A. Rajoriya, and R. Budhiraja, "Near-field channel estimation for XL-MIMO systems using variational bayesian learning," *IEEE Trans. Wireless Commun.*, vol. 23, no. 9, pp. 10 740 – 10 756, Sep. 2024.
- [133] X. Xie, Y. Wu, J. An, D. W. K. Ng, C. Xing, and W. Zhang, "Massive unsourced random access for near-field communications," *IEEE Trans. Commun.*, Early Access 2024.
- [134] K. Arai, K. Ishibashi, H. Iimori, P. V. Klaine, and S. Malomosky, "Near-field channel estimation for uplink multiuser XL-MIMO systems," in *2024 IEEE 25th International Workshop on Signal Processing Advances in Wireless Communications (SPAWC)*. IEEE, 2024, pp. 256–260.
- [135] L. V. Nguyen, D. H. Nguyen, I. Atzeni, A. Tölili, and A. L. Swindlehurst, "Channel estimation in low-resolution near-field massive MIMO systems," in *2024 IEEE 13rd Sensor Array and Multichannel Signal Processing Workshop (SAM)*. IEEE, 2024, pp. 1–5.
- [136] Y. Chen and L. Dai, "Non-stationary channel estimation for extremely large-scale MIMO," *IEEE Trans. Commun.*, vol. 23, no. 7, pp. 7683 – 7697, Jul. 2024.
- [137] X. Zhang and J. Zheng, "Non-stationary near-field channel estimation for XL-MIMO systems with hybrid combining," *IEEE Wirel. Commun. Lett.*, vol. 13, no. 10, pp. 2727 – 2731, Oct. 2024.
- [138] S. Jiang and C. Lee, "Near-field channel estimation for hybrid massive MIMO-OFDM systems," in *2024 International Conference on Electronics, Information, and Communication (ICEIC)*. IEEE, 2024, pp. 1–4.
- [139] X. Zhang, H. Zhang, and Y. C. Eldar, "Near-field sparse channel representation and estimation in 6G wireless communications," *IEEE Trans. Commun.*, vol. 72, no. 1, p. 450–464, Oct. 2024.
- [140] A. Hussain, A. Abdallah, and A. M. Eltawil, "Near-field channel estimation for ultra-massive MIMO antenna array with hybrid architecture," in *2024 IEEE Wireless Communications and Networking Conference (WCNC)*. IEEE, 2024, pp. 1–6.
- [141] C. Ruan, Z. Zhang, H. Jiang, J. Dang, L. Wu, and H. Zhang, "Wideband near-field channel covariance estimation for XL-MIMO systems in the face of beam split," *IEEE Trans. Veh. Technol.*, 2024.
- [142] A. M. Elbir, K. V. Mishra, and S. Chatzinotas, "NBA-OMP: Near-field beam-split-aware orthogonal matching pursuit for wideband thz channel estimation," in *Proc. IEEE ICASSP*. IEEE, 2023, pp. 1–5.

- [143] M. Cui and L. Dai, "Near-field wideband channel estimation for extremely large-scale MIMO," *Sci. China. Inf. Sci.*, vol. 66, no. 7, p. 172303, Jun. 2023.
- [144] N. Chen, S. Li, and B. Su, "A segmented off-grid near-field wideband channel estimation approach for XL-MIMO," in *2024 7th World Conference on Computing and Communication Technologies (WCCCT)*. IEEE, 2024, pp. 152–157.
- [145] S. Jang and C. Lee, "Neural network-aided near-field channel estimation for hybrid beamforming systems," *IEEE Trans. Commun.*, vol. 72, no. 11, pp. 6768 – 6782, Nov. 2024.
- [146] P. Zheng, X. Lyu, Y. Wang, and Y. Gong, "Dictionary learning based near-field channel estimation for wideband XL-MIMO systems," in *2024 IEEE 25th International Workshop on Signal Processing Advances in Wireless Communications (SPAWC)*. IEEE, 2024, pp. 246–250.
- [147] A. M. Elbir, W. Shi, A. K. Papazafeiropoulos, P. Kourtessis, and S. Chatzinotas, "Near-field terahertz communications: Model-based and model-free channel estimation," *IEEE Access*, vol. 11, pp. 36 409–36 420, 2023.
- [148] Z. Jin, L. You, D. W. Kwan Ng, X.-G. Xia, and X. Gao, "A generative denoising approach for near-field XL-MIMO channel estimation," in *GLOBECOM 2024 - 2024 IEEE Global Communications Conference*, 2024, pp. 3443–3448.
- [149] Q. Ruan and J. Zheng, "Channel estimation of uplink extremely large-scale MIMO in wideband near-field communications," in *2024 International Conference on Ubiquitous Communication (Ucom)*. IEEE, 2024, pp. 163–168.
- [150] H. Wu, L. Lu, and Z. Wang, "Near-field channel estimation in dual-band XL-MIMO with side information-assisted compressed sensing," *IEEE Trans. Commun.*, vol. 72, no. 7, pp. 1353 – 1366, Feb. 2025.
- [151] X. Yu, W. Shen, R. Zhang, C. Xing, and T. Q. S. Quek, "Channel estimation for XL-RIS-aided millimeter-wave systems," *IEEE Trans. Commun.*, vol. 71, no. 9, pp. 5519–5533, 2023.
- [152] Z. Lu, Y. Han, J. Wang, J. Zhang, and S. Jin, "Low-overhead separate channel estimation for hybrid XL-RIS-aided MIMO systems," *IEEE Trans. Commun.*, 2024.
- [153] R. Schroeder, J. He, H. Djelouat, and M. Juntti, "Low-complexity near-field channel estimation for hybrid RIS assisted systems," in *2024 IEEE 13rd Sensor Array and Multichannel Signal Processing Workshop (SAM)*. IEEE, 2024, pp. 1–5.
- [154] J. Lee and S. Hong, "Two-timescale channel estimation for RIS-aided near-field communications," *arXiv preprint arXiv:2501.02985*, 2025.
- [155] O. Rinchi, A. Elzanaty, and M.-S. Alouini, "Compressive near-field localization for multipath RIS-aided environments," *IEEE Commun. Lett.*, vol. 26, no. 6, pp. 1268–1272, Jun. 2022.
- [156] J. Wu, S. Kim, and B. Shim, "Parametric sparse channel estimation for RIS-assisted terahertz systems," *IEEE Trans. Commun.*, vol. 71, no. 9, pp. 5503–5518, Sep. 2023.
- [157] Y. Du, Y. Hu, F. Zhang, V. G. Menon, and B. Ji, "Three-dimensional channel estimation for near-field XL-RIS: A polar-domain approach," *IEEE Trans. Consum. Electron.*, early access, 2025.
- [158] S. Yang, C. Xie, W. Lyu, B. Ning, Z. Zhang, and C. Yuen, "Near-field channel estimation for extremely large-scale reconfigurable intelligent surface (XL-RIS)-aided wideband mmwave systems," *IEEE J. Sel. Areas Commun.*, vol. 42, no. 6, pp. 1567 – 1582, 2024.
- [159] Y. Han, S. Jin, C.-K. Wen, and T. Q. Quek, "Localization and channel reconstruction for extra large RIS-assisted massive MIMO systems," *IEEE J. Sel. Top. Signal Process.*, vol. 16, no. 5, pp. 1011–1025, Aug. 2022.
- [160] J. Chen, Y.-C. Liang, H. V. Cheng, and W. Yu, "Channel estimation for reconfigurable intelligent surface aided multi-user mmwave MIMO systems," *IEEE Trans. Wireless Commun.*, vol. 22, no. 10, pp. 6853–6869, Oct. 2023.
- [161] Y. Wang, Y. Li, M. Chen, Y. Yao, F. Shu, and J. Wang, "Enhanced channel estimation for near-field IRS-aided multi-user MIMO system via deep residual network," *arXiv preprint arXiv:2410.20992*, 2024.
- [162] Z. Wang, L. Liu, and S. Cui, "Channel estimation for intelligent reflecting surface assisted multiuser communications: Framework, algorithms, and analysis," *IEEE Trans. Commun.*, vol. 19, no. 10, pp. 6607–6620, Oct. 2020.
- [163] S. Yang, W. Lyu, Z. Hu, Z. Zhang, and C. Yuen, "Channel estimation for near-field XL-RIS-aided mmwave hybrid beamforming architectures," *IEEE Trans. Veh. Technol.*, vol. 72, no. 8, pp. 11 029–11 034, Aug. 2023.
- [164] Y. Pan, C. Pan, S. Jin, and J. Wang, "RIS-aided near-field localization and channel estimation for the terahertz system," *IEEE J. Sel. Topics Signal Process.*, vol. 17, no. 4, pp. 878–892, Jun. 2023.
- [165] R. Chen, J. He, J. Cao, H. Lin, and Z. Yu, "A novel near-field channel estimation method for RIS-assisted UM-MIMO systems," in *Proc.Int.Conf.Culture-Oriented Sci.Technol. (CoST)*. IEEE, 2023, pp. 277–281.